B.8.2.5 Uncertainty in Anchor Point Time (t_1)

Uncertainty in the Weibull model is incorporated through the Weibull intercept parameter, and no anchor point is defined. The Weibull intercept parameter uncertainty is estimated by linearizing the Weibull model form and performing regression to the time to first crack data for RPVHPNs. To make a prediction with the model, the Weibull intercept parameter uncertainty is incorporated, effectively defining a Weibull characteristic time. Then, the initiation time is sampled from the Weibull distribution defined by the Weibull slope and characteristic time parameters.

B.8.2.6 Uncertainty in the Multiple Flaw Weibull Slope

As discussed in the modeling section, a second Weibull model is used to predict the initiation of multiple flaws on a single head. The key input to this model is the Weibull slope.

The slope of the multiple flaw Weibull model, β_{flaw}, quantifies the rate at which flaws occur after the initiation of the first flaw. An analytical data fitting procedure, as done for the first initiation time model, was not considered appropriate to fit β_{flaw} given the modeling complexities involved in sampling multiple flaw initiation times. Instead, a mean value of 2.0 was selected for the β_{flaw}. This value has a precedent in probabilistic modeling of SCC in steam generators [14]. A normal distribution with a mean of 2.0 and a standard deviation of 0.5 is employed to incorporate uncertainties due to material and manufacturing disparities. A lower truncation bound of 1.0 was selected to preclude a multiple flaw Weibull model in which the PWSCC initiation rate decreases over time.

A numerical experiment was run with a value of 2.0 for β_{flaw} in order to demonstrate the resulting number of cracks per head, given the parameter distributions discussed throughout this Section B.8. Figure B-18 depicts the resulting distribution of number of flaws in heads with at least a single flaw, at 21.5 EFPY, given an operating temperature of 605°F. The average number of flaws at 21.5 EFPY, given that at least a single flaw exists, is 20.9. This average number of flaws approximately matches industry data (depicted in Figure B-19) for which the average number of cracking indications per hot head with at least one cracking indication was 15.1.

To account for undetected flaws in industry, namely those located on the J-groove welds, a sensitivity study will be included in which the multiple flaw Weibull model is increased, resulting in a higher average number of flaws per head with at least one flaw.

B.8.2.7 Uncertainty in Initial Flaw Location

As discussed in the modeling section, an initial flaw location is required for OD axial flaws. This initial flaw location, together with the sampled weld toe to weld root distance, defines the OD axial crack half-length that would result in the opening of the OD nozzle annulus (i.e., leakage).

For each initiated OD axial flaw, the flaw center location is uniformly sampled between the weld toe and the location where the residual stresses in the penetration nozzle fall below 80% of yield stress. The distance from the weld toe to the 80% yield location (the "80% yield stress length") is taken as a distributed input and is fit to results of finite analysis of J-groove welding residual

stresses [6]. The variation in the 80% yield stress length is due to process variation and geometrical variation across different penetration nozzle incidence angles[16].

A unique normal distribution was used for the uphill and downhill sides of the penetration. The resulting fits are shown in Figure B-20 and Figure B-21. The distribution parameters are given in Table B-5.

B.8.2.8 Uncertainty in Initial Flaw Depth

The initial through-wall fraction for each flaw location is sampled at the time of flaw initiation. To remain consistent with the initial through-wall fractions used in the DM weld program (which are based on experimental data for UT inspection of cracking in DM welds), a log-normal distribution with a median of 5% through-wall and an upper 95% confidence bound of 9% through-wall is used. For the penetration nozzle thickness presented earlier (15.9 mm) this results in a median absolute initiation depth of 0.8 mm.

The lower truncation limit was defined to prevent the initiation of very small flaws for which the stress intensity factor (based on the input distributions of the surface welding residual stress) would be significantly less than the range of stress intensity factors (about 15-20 MPa-$m^{1/2}$ or 14-18 ksi-$in^{1/2}$) evaluated in the laboratory studies used to define the flaw propagation models given in MRP-55.

A sensitivity case is used to explore an initial depth distribution that results in cracks that initiate approximately 5 times smaller. This is included to assess the potential effect on leakage probability of smaller cracks not being identified during inspections prior to peening.

A second sensitivity study is presented in which cracks initiate with the same *absolute* depths (as opposed to through-wall percentages) used for the DM weld program.

B.8.2.9 Uncertainty in Flaw Aspect Ratio

There was not enough data available for initial RPVHPN crack sizes to allow a distribution to be fit for aspect ratio, as was done for DM weld cracks. Instead, a log-normal distribution was applied to give a modal aspect ratio of 4.0 and a 99% confidence interval aspect ratio of 10.0.

B.8.2.10Uncertainty in Temperature Effect

The uncertainty in temperature and its effect on initiation is handled in same manner as described for DM welds in Section A.8.2.10.

[16] Trends in the 80% yield stress length as a function of penetration incidence angle were analyzed. The trends were not strong enough to justify their implementation in this study.

Table B-5
Summary of Inputs for RPVHPN Initiation Model

Symbol	Description	Source	Units	Parameter Type	Hot Head Base Case	Cold Head Base Case
t_1	Time at which failure fraction F_1 is reached on RPVHPNs	Flaw initiation data assessed in MRP–395	EDY		23.0	23.0
σ_c	Standard error in intercept of linearized Weibull fit	Linearized Weibull fit to flaw initiation data assessed in MRP–395	ln(EDY)		0.2705	0.2705
F_1	Arbitrary failure fraction selected to define Weibull PWSCC initiation function	Selected to reflect t_1 as the Weibull scale parameter (characteristic time)	-		0.6321	0.6321
β	Weibull slope for PWSCC flaw initiation on RPVHPNs	Flaw initiation data assessed in MRP–395	-		1.379	1.379
β_{flaw}	Weibull slope for PWSCC multiple flaw initiation on RPVHPNs	Based on representative value for formation of PWSCC at multiple locations in industry SGs	-	type	Normal	Normal
				mean	2.0	2.0
				stdev	0.5	0.5
				min	1.0	1.0
				max	5.0	5.0
ρ_{heat}	Correlation coefficient for PWSCC initiation and propagation of all cracks in Alloy 600	xLPR Input	-		0.0	0.0
ρ_{weld}	Correlation coefficient for PWSCC initiation and propagation of all cracks in Alloy 82/182 weld	xLPR Input	-		0.0	0.0

Table B-5 (continued)
Summary of Inputs for RPVHPN Initiation Model

Symbol	Description	Source	Units	Parameter Type	Hot Head Base Case	Cold Head Base Case
Q_i	Thermal activation energy for PWSCC flaw initiation	Distribution based on laboratory data and experience with Weibull analysis	kcal/mole	type	Normal	Normal
				mean	44.03	44.03
				stdev	3.06	3.06
				min	25.65	25.65
				max	62.41	62.41
$T_{ref,i}$	Reference temperature to normalize PWSCC flaw initiation data	Temperature used to adjust flaw initiation data assessed in this report	°R		1060	1060
a_0	Initial depth assigned to newly initiated flaw	Consistency with initial through-wall fractions of DM weld model	in.	type	Log-Normal	Log-Normal
				linear μ	3.32E-02	3.32E-02
				median	3.12E-02	3.12E-02
				log-norm μ	-3.47	-3.47
				log-norm σ	0.35	0.35
				min	0.02	0.02
				max	0.62	0.62
AR	General initial aspect ratio assigned to newly initiated flaw	Based on aspect ratios of PWSCC cracks observed in inspections of DMW and RPVHPN components	-	type	Log-Normal	Log-Normal
				linear μ	4.77	4.77
				median	4.50	4.50
				log-norm μ	1.50	1.50
				log-norm σ	0.34	0.34
				min	0.57	0.57
				max	35.20	35.20
	Distance from weld toe to location where welding residual stress is equal to 80% of yield stress, uphill side	Finite element analyses of J–groove weld residual stresses; across various units and penetration geometries	in.	type	Normal	Normal
				mean	0.25	0.25
				stdev	0.13	0.13
				min	0.00	0.00
				max	1.03	1.03
	Distance from weld toe to location where welding residual stress is equal to 80% of yield stress, downhill side	Finite element analyses of J–groove weld residual stresses; across various units and penetration geometries	in.	type	Normal	Normal
				mean	0.24	0.24
				stdev	0.06	0.06
				min	0.00	0.00
				max	0.61	0.61

Table B-6
Inspection Data Through Fall 2013 Extrapolated Back to Predicted Time to First Crack/Leak (Based on Weibull slope β = 3) [3]

				NDE Date, Scope, and Results										
							All Nozzle Materials						at Detection of Cracking	at 1st Crack Extrapolated Back using b=3
Code	No. CRDM/ CEDM Nozzles	Replace Date		Outage	Year	EDY	NDE CRDM/ CEDM	Cum. Cracked	CDF (1st Crack)	CDF (# Cracked)	Time Factor (# Cracked)	EDYs at 1st Crack or Inspection (+8°F for all B&W Heads)	CDF of Units with Cracks (+8°F for all B&W Heads)	CDF of Units with Cracks (+8°F for all B&W Heads)
Plant A	78			Fall	2006	2.56	78	0	0.0089			2.5559		
Plant B	78			Spring	2011	2.63	78	0	0.0089			2.6252		
Plant C	65	Spring	2007	Spring	2005	16.67	65	0	0.0107			16.6688		
Plant D	78			Fall	2012	3.87	78	0	0.0089			3.8692		
Plant E	69	Fall	2003	Spring	2002	23.16	23	5	0.0299	0.2009	0.5136	16.3672	0.86	0.45
Plant F	78			Fall	2012	4.30	78	0	0.0089			4.3015		
Plant G	78	Spring	2005	NONE			0	0	1.7500					
Plant H	45			Spring	2009	12.05	45	2	0.0154	0.0374	0.7412	8.9293	0.15	0.20
Plant I	78	Fall	2014	Spring	2007	3.21	78	0	0.0089			3.2092		
Plant J	78			Spring	2013	19.09	78	0	0.0089			19.0900		
Plant K	65	Spring	2006	Fall	2004	15.01	65	4	0.0107	0.0566	0.5696	8.5493	0.23	0.16
Plant L	78			Spring	2013	4.00	78	0	0.0089			3.9989		
Plant M	65	Fall	2004	Spring	2003	18.17	65	0	0.0107			18.1659		
Plant N	78			Fall	2011	2.61	78	1	0.0089	0.0089	1.0000	2.0854	0.01	0.04
Plant O	65	Spring	2003	Fall	2001	19.89	30	1	0.0230	0.0230	1.0000	19.8859	0.44	0.56
Plant P	65	Spring	2003	Fall	2001	19.12	16	6	0.0427	0.3476	0.4675	8.9394	0.34	0.22
Plant Q	65	Spring	2017	Fall	2009	14.84	65	2	0.0107	0.0260	0.7420	11.0115	0.20	0.33
Plant R	97	Fall	2009	Spring	2008	14.65	97	0	0.0072			14.6502		
Plant S	81			Fall	2013	19.10	81	0	0.0086			19.1000		
Plant T	97	Fall	2010	Spring	2009	15.19	97	0	0.0072			15.1860		
Plant U	91			Fall	2008	18.74	91	0	0.0077			18.7386		
Plant V	69	Fall	2011	Spring	2010	9.17	69	12	0.0101	0.1686	0.3801	3.4853	0.11	0.10
Plant W	78			Spring	2013	3.54	78	0	0.0089			3.5400		
Plant X	65			Fall	2013	4.00	65	6	0.0107	0.0872	0.4905	1.9615	0.07	0.03
Plant Y	78			Spring	2008	1.76	78	0	0.0089			1.7611		
Plant Z	74	Fall	2009	Fall	2006	11.70	74	0	0.0094			11.7029		
Plant AA	65	Spring	2005	Fall	2003	18.50	65	0	0.0107			18.4957		
Plant AB	78	Fall	2007	Spring	2006	14.43	78	1	0.0089	0.0089	1.0000	10.1300	0.13	0.27
Plant AC	40	Fall	2004	NONE			0	0	1.7500					
Plant AD	69	Spring	2004	Fall	2002	23.61	69	19	0.0101	0.2695	0.3184	10.3475	0.93	0.29
Plant AE	79	Fall	2005	Spring	2004	12.90	79	0	0.0088			12.8951		
Plant AF	40	Spring	2005	NONE			0	0	1.7500					
Plant AG	78			Fall	2012	3.94	78	0	0.0089			3.9403		
Plant AH	79	Fall	2010	Spring	2009	13.24	79	0	0.0088			13.2412		
Plant AI	78			Spring	2012	3.11	78	1	0.0089	0.0089	1.0000	3.1055	0.05	0.08

Table B-6 (continued)
Inspection Data Through Fall 2013 Extrapolated Back to Predicted Time to First Crack/Leak (Based on Weibull slope β = 3) [3]

				NDE Date, Scope, and Results											
							All Nozzle Materials						at Detection of Cracking	at 1st Crack Extrapolated Back using b=3	
Code	No. CRDM/ CEDM Nozzles	Replace Date		Outage	Year	EDY	NDE CRDM/ CEDM	Cum. Cracked	CDF (1st Crack)	CDF (# Cracked)	Time Factor (# Cracked)	EDYs at 1st Crack or Inspection (+8°F for all B&W Heads)	CDF of Units with Cracks (+8°F for all B&W Heads)	CDF of Units with Cracks (+8°F for all B&W Heads)	
Plant AJ	65	Fall	2003	NONE			0	0	1.7500						
Plant AK	78			Spring	2011	2.76	78	4	0.0089	0.0472	0.5703	1.5747	0.03	0.01	
Plant AL	69	Fall	2003	Fall	2001	16.20	9	1	0.0745	0.0745	1.0000	22.3057	0.51	0.71	
Plant AM	78			Fall	2007	1.94	78	0	0.0089			1.9383			
Plant AN	69	Fall	2004	Spring	2003	17.46	69	0	0.0101			17.4581			
Plant AO	49	Spring	2005	Fall	2003	16.60	49	0	0.0142			16.5959			
Plant AP	40	Spring	2006	NONE			0	0	1.7500						
Plant AQ	65	Spring	2003	Fall	2002	19.71	65	45	0.0107	0.6835	0.2107	4.1523	0.39	0.12	
Plant AR	69	Fall	2003	Fall	2001	18.08	12	8	0.0565	0.6210	0.3913	9.7426	0.58	0.24	
Plant AS	78			Spring	2011	3.11	77	0	0.0090			3.1111			
Plant AT	78	Spring	2007	NONE			0	0	1.7500						
Plant AU	78			Fall	2013	3.79	78	0	0.0089			3.7900			
Plant AV	69	Fall	2005	Spring	2004	21.69	69	0	0.0101			21.6900			
Plant AW	78			Spring	2013	4.08	78	0	0.0089			4.0800			
Plant AX	79	Fall	2006	Spring	2005	8.70	79	0	0.0088			8.7004			
Plant AY	69	Fall	2005	Spring	2004	16.70	69	0	0.0101			16.7000			
Plant AZ	78			Fall	2006	1.86	78	0	0.0089			1.8551			
Plant BA	91	Fall	2012	Fall	2009	19.78	91	0	0.0077			19.7833			
Plant BB	37	Fall	2003	NONE			0	0	1.7500						
Plant BC	97	Spring	2010	Fall	2008	15.29	97	0	0.0072			15.2946			
Plant BD	78			Spring	2013	4.02	78	0	0.0089			4.0200			
Plant BE	69	Fall	2005	Spring	2004	16.80	69	0	0.0101			16.8000			
Plant BF	97			Spring	2012	12.70	97	0	0.0072			12.7000			
Plant BG	78	Fall	2009	Spring	2008	14.37	78	0	0.0089			14.3701			
Plant BH	91	Fall	2007	Spring	2006	16.40	91	5	0.0077	0.0514	0.5261	8.6281	0.28	0.18	
Plant BI	65	Spring	2006	Spring	2004	16.42	65	0	0.0107			16.4150			
Plant BJ	69	Fall	2005	Spring	2004	22.62	69	8	0.0101	0.1110	0.4417	13.7499	0.79	0.36	
Plant BK	49	Fall	2005	Spring	2004	15.50	49	1	0.0142	0.0142	1.0000	15.5000	0.25	0.42	
Plant BL	69	Fall	2003	Spring	2002	26.50	69	5	0.0101	0.0677	0.5248	13.9070	0.65	0.39	
Plant BM	74	Spring	2010	Spring	2007	12.19	74	0	0.0094			12.1918			
Plant BN	91	Fall	2012	Fall	2012	24.68	91	0	0.0077			24.6800			
Plant BO	69	Spring	2005	Fall	2003	12.36	69	14	0.0101	0.1974	0.3586	4.4309	0.17	0.14	
Plant BP	41	Fall	2006	Spring	2005	13.09	41	0	0.0169			13.0947			
Plant BQ	69	Spring	2003	Fall	2001	22.39	69	16	0.0101	0.2262	0.3406	10.4982	0.72	0.31	
Plant BR	65			Fall	2012	4.08	65	4	0.0107	0.0566	0.5696	2.3210	0.09	0.06	

Table B-7
Summary of Weibull Probability Distribution Parameter Fitting for RPVHPN Analysis

Fitting Method	β	θ (EDY)	Standard Error in Vertical Intercept (ln(EDY))
Linearized Least Squares	1.379	23	0.2705

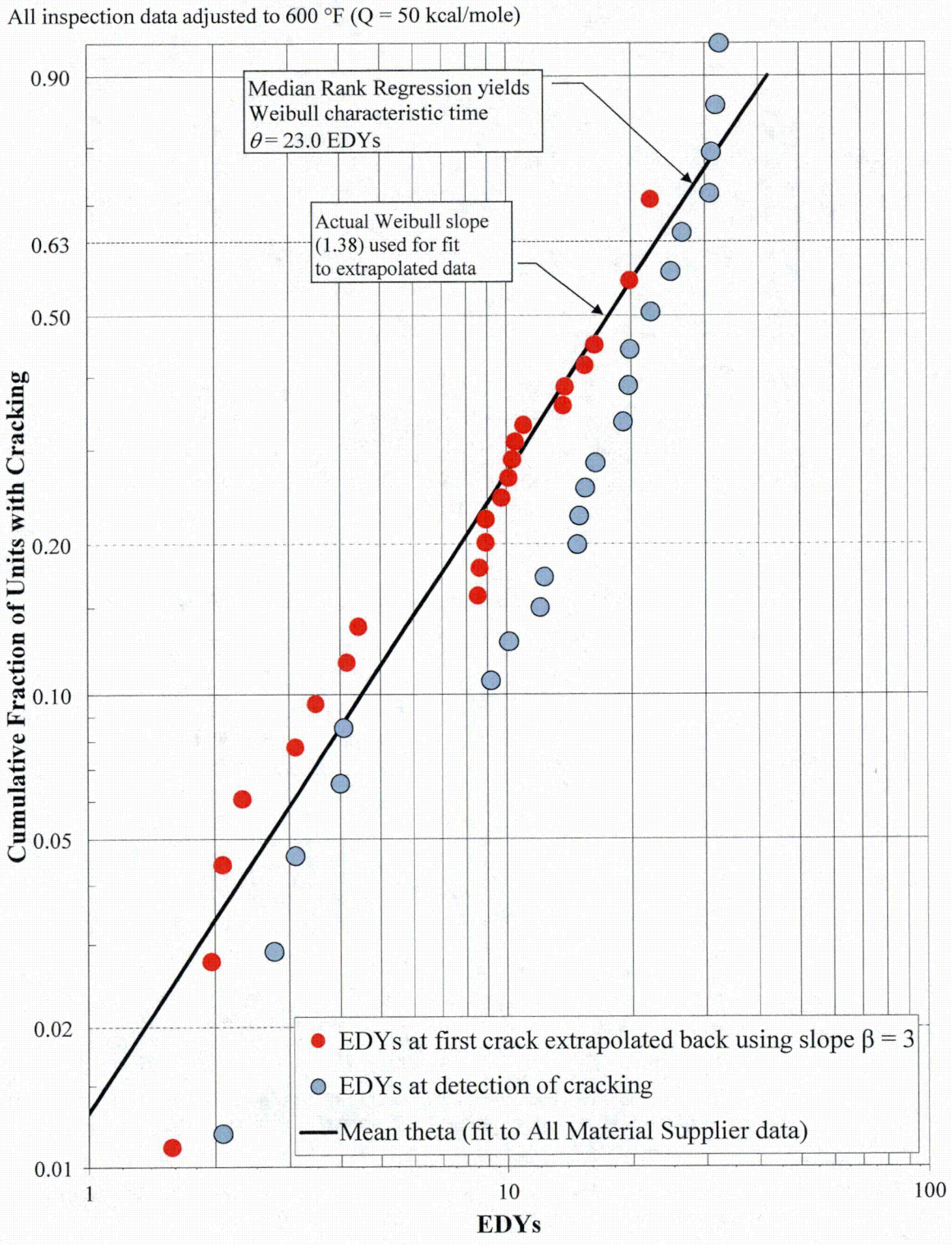

Figure B-17
Example MLE Weibull Probability Distribution for Alloy 600 RPVHPNs with Alloy 82/182 J-groove Welds

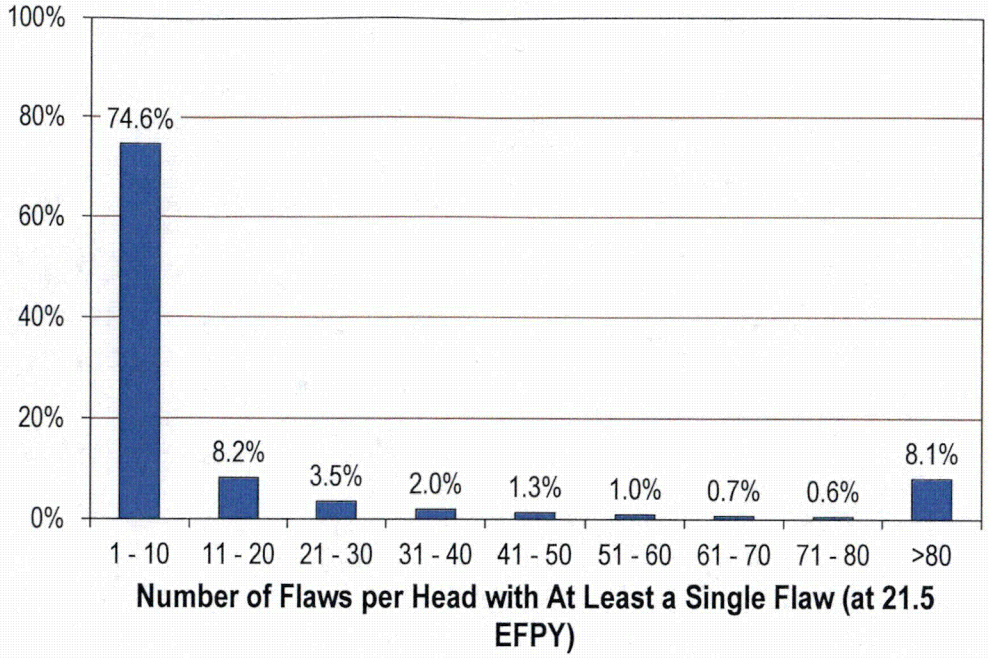

Figure B-18
Result of RPVHPN Numerical Initiation Study: Distribution of Number of Flaws per Hot Head with at Least a Single Flaw

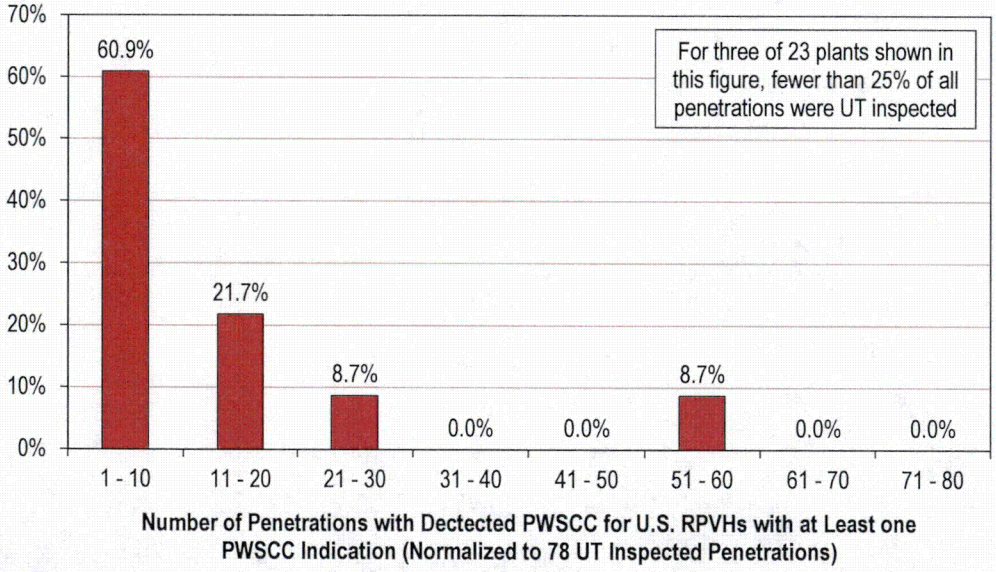

Figure B-19
Industry RPVHPN Flaw Initiation Data: Distribution of Normalized Number of Nozzles with PWSCC Indications per Head with at Least a Single Indication (23 Plants)

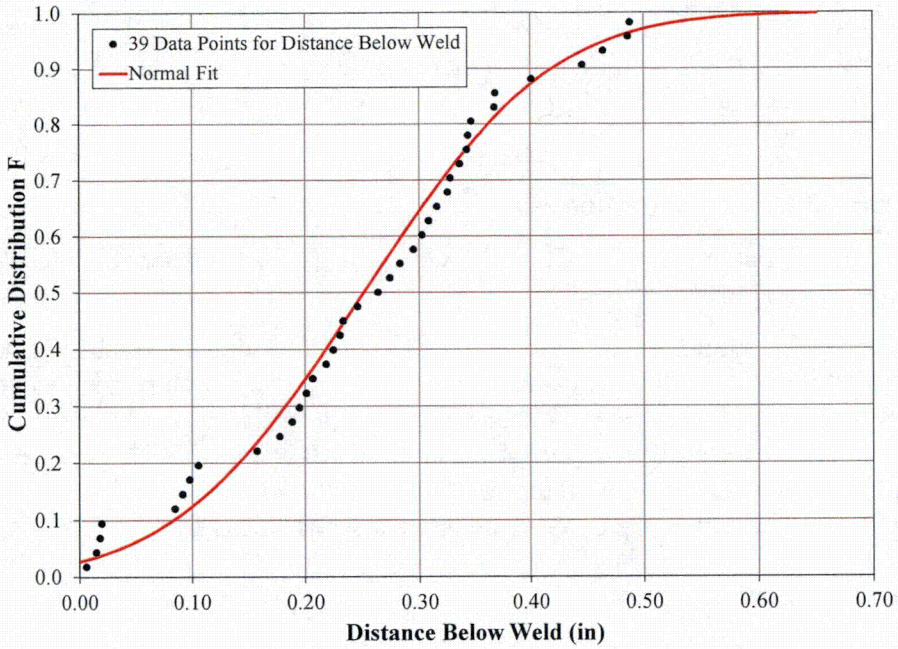

Figure B-20
Normal Distribution Fit to 80% Yield Stress Length on Uphill Side of Penetration Predicted by Different FEA Studies

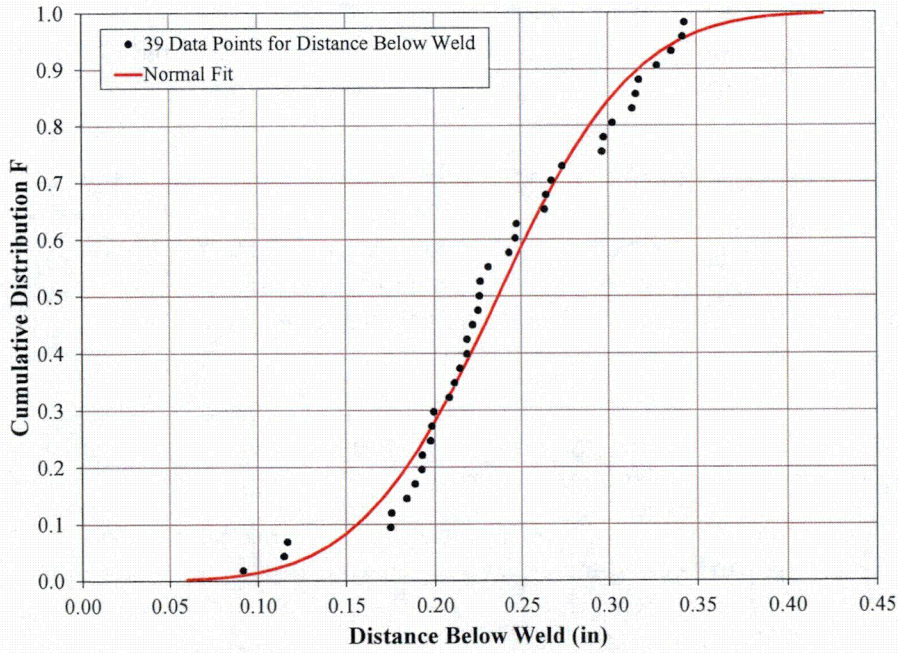

Figure B-21
Normal Distribution Fit to 80% Yield Stress Length on Downhill Side of Penetration Predicted by Different FEA Studies

B.8.3 Crack Growth Model

The set of inputs for the PWSCC propagation model is described in Table B-8 at the end of this section, including deterministic and distributed inputs. Various inputs are detailed in the following subsections.

B.8.3.1 Empirical Growth Parameters

The empirical growth parameters for Alloy 82/182 weld cracks are identical to those used for the DM weld program (see Section A.8.3.1).

The empirical growth parameters for Alloy 600 are based on the crack growth data compiled and presented in MRP-55 [12]. Instead of using a crack growth curve with a stress intensity factor threshold of 9 MPa-$m^{1/2}$ and power law exponent of 1.16 (as suggested in MRP-55), a more bounding curve with a stress intensity factor threshold of 0.0 and power law exponent of 1.6 is fit to the data. Both curves are shown with the Alloy 600 CGR data in Figure B-22. The parameters for Alloy 600 curve that will be used in this study are given Table B-8.

B.8.3.2 Growth Variation Factors

The growth variation factor for Alloy 82/182 weld cracks are identical to those used for the DM weld program (see Section A.8.3.2).

Similar to the way growth uncertainty is accounted for in the weld material, the uncertainty of flaw propagation in Alloy 600 is characterized by f_{heat} and f_{wh} parameters.

The f_{heat} parameter is a common factor applied to all specimens fabricated from the same raw material to account for the effects of manufacturing variation. For this study, a log-normal distribution is fit to the heat factors for 26 laboratory heat specimens assessed in MRP-55 (see Figure B-23).

A "within-heat factor" (f_{wh}) describes the variability in flaw propagation rate for different Alloy 600 specimens from the same raw material (heat). A log-normal distribution was developed to describe the variability in f_{wh} for the data generated in MRP-55. The f_{wh} distribution describes the scatter in the flaw propagation rate model that remain after all effects addressed by the model are considered including the particular f_{heat} parameter calculated for the test heat. For this study, a log-normal distribution is fit to the heat factors for 140 laboratory crack specimens assessed in MRP-55 (see Figure B-24).

The lower and upper bounds for the growth variability distributions are set in the same manner as described for DM weld growth variation factors.

In addition to the heat-to-heat and within-heat variation terms, other forms of uncertainty are incorporated for the growth of circumferential through-wall cracks, as discussed in the modeling section.

- First, for the random multiplicative factor used to scale the FEA-derived K curves, a triangular distribution with a minimum and mode of 1.0 and a maximum of 2.0 is used. This results in a modestly increased K curve to account for any non-conservative bias in the FEA results.

- Second, for the environmental factor that scales the length growth rate predicted by the Alloy 600 CGR curve, a triangular distribution with a minimum and mode of 1.0 and a maximum of 2.0 is used. Based on the consensus of the international PWSCC expert panel convened by EPRI in 2001-2002, the crack growth rate for flaws connected to the OD annulus environment is most likely not significantly accelerated due to chemical concentration effects. However, as documented in MRP-55 [12], the expert panel conservatively recommended an environmental factor of 2 for deterministic calculations of growth of circumferential flaws in contact with the annulus environment. The triangular distribution described above was selected based on this work.

B.8.3.3 Uncertainty in Temperature Effect

The uncertainty in temperature and its effect on propagation is handled in same manner as described for DM welds in Section A.8.3.3.

B.8.3.4 Correlation in Relating Flaw Initiation and Propagation

As done for DM welds, the correlation in relating flaw initiation and propagation is not included for base case analysis.

Table B-8
Summary of Inputs for RPVHPN Flaw Propagation Model

Symbol	Description	Source	Units	Parameter Type	Hot Head Base Case	Cold Head Base Case
$1/\Delta t$	Number of time steps per year for crack size increment	The value chosen provides sufficient convergence	1/yr		12	12
f_{heat}	Heat-to-heat factor: common factor applied to all specimens fabricated from the same material to account for manufacturing variations	Fit to heat-to-heat variation data from MRP-55	-	type	Log-normal	Log-Normal
				linear μ	1.68	1.68
				median	1.00	1.00
				75%ile	1.98	1.98
				log-norm μ	0.00	0.00
				log-norm σ	1.016	1.016
				min	0.14	0.14
				max	5.32	5.32
f_{wh}	Within-heat factor: factor accounting for the variability in crack growth rate for different specimens fabricated from the same raw material	Fit to within-heat variation from MRP-55 data after normalizing for heat-to-heat variation factor	-	type	Log-Normal	Log-Normal
				linear μ	1.18	1.18
				median	1.00	1.00
				log-norm μ	0.00	0.00
				log-norm σ	0.5695	0.5695
				min	0.21	0.21
				max	3.68	3.68
f_{weld}	Weld-to-weld factor: common factor applied to all specimens fabricated from the same weld to account for weld wire/stick heat processing and for weld fabrication	Fit to weld-to-weld variation data from MRP-115	-	type	Log-Normal	Log-Normal
				linear μ	1.19	1.19
				median	1.00	1.00
				75%ile	1.49	1.49
				log-norm μ	0.00	0.00
				log-norm σ	0.5892	0.5892
				min	0.313	0.313
				max	2.64	2.64
f_{ww}	Within-weld factor: factor accounting for the variability in crack growth rate for different specimens fabricated from the same weld	Fit to within-weld variation from MRP-115 data after normalizing for weld-to-weld variation factor	-	type	Log-Normal	Log-Normal
				linear μ	1.12	1.12
				median	1.00	1.00
				log-norm μ	0.00	0.00
				log-norm σ	0.4807	0.4807
				min	0.309	0.309
				max	3.24	3.24

Table B-8 (continued)
Summary of Inputs for RPVHPN Flaw Propagation Model

Symbol	Description	Source	Units	Parameter Type	Hot Head Base Case	Cold Head Base Case
α_{heat}	Flaw propagation rate equation power law constant for Alloy 600	Fit to MRP-55 data with power law constant of 1.6 and stress intensity factor threshold of zero	(in/hr)/(ksi-in.$^{0.5}$)$^{1.6}$		3.25E-08	3.25E-08
α_{weld}	Flaw propagation rate equation power law constant for Alloy 182 weld	MRP-115	(in/hr)/(ksi-in.$^{0.5}$)$^{1.6}$		1.62E-07	1.62E-07
Q_g	Thermal activation energy for PWSCC flaw propagation	MRP-115	kcal/mole	type	Normal	Normal
				mean	31.07	31.07
				stdev	1.20	1.20
				min	23.90	23.90
				max	38.24	38.24
$T_{ref,g}$	Absolute reference temperature to normalize PWSCC flaw propagation data	MRP-55, MRP-115	°R		1077	1077
$K_{I,th,heat}$	Flaw propagation rate equation power law threshold for Alloy 600	Conservatively assumed threshold such that all cracks with positive K_I have a non-zero crack growth rate	ksi-in.$^{0.5}$		0.0	0.0
$K_{I,th,weld}$	Flaw propagation rate equation power law threshold for Alloy 82/182 weld	MRP-115	ksi-in.$^{0.5}$		0.0	0.0
$K_{I,min,heat}$	Minimum allowable K_I value for Alloy 600 components	No technical basis for non-zero value	ksi-in.$^{0.5}$		0.0	0.0
$K_{I,min,weld}$	Minimum allowable K_I value for Alloy 182 components	No technical basis for non-zero value	ksi-in.$^{0.5}$		0.0	0.0
n_{heat}	Flaw propagation rate equation power law exponent for Alloy 600	Fit to MRP-55 data with stress intensity factor threshold of zero	-		1.6	1.6
n_{weld}	Flaw propagation rate equation power law exponent for Alloy 182 weld	MRP-115	-		1.6	1.6
	Flag indicating if crack growth will be predicted considering the effect of crack closure	Crack closure effects are neglected for base case	Logical		FALSE	FALSE
	Flag indicating if cracks may grow in length without the effect of peening stresses	Approximates sub-surface balloon growth of crack	Logical		TRUE	TRUE

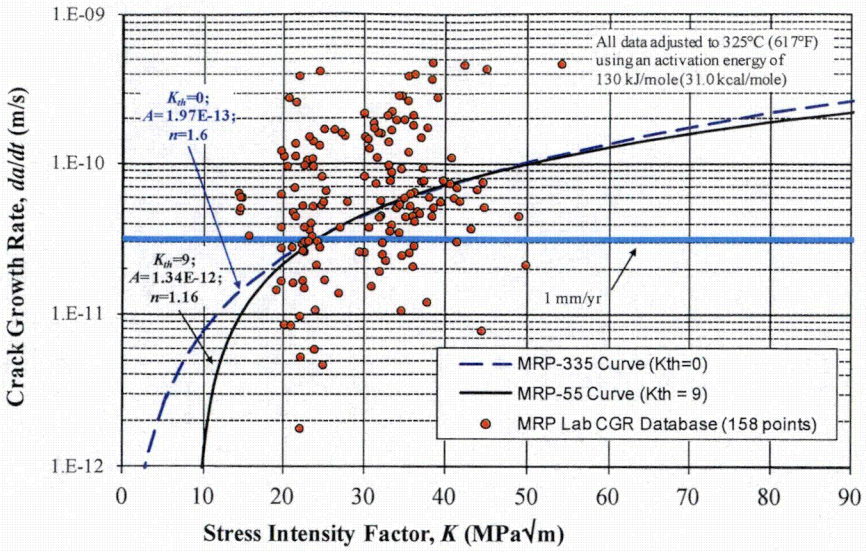

Figure B-22
Alloy 600 Crack Growth Rate Curves: MRP-55 (K_{Ith}=9) Curve and MRP-335 (K_{Ith}=0) Curve

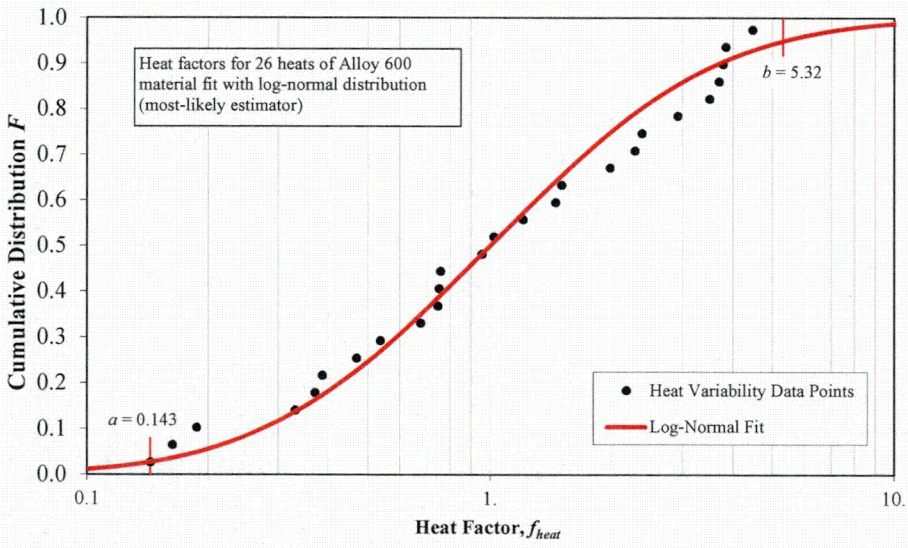

Figure B-23
Heat Factor f_{heat} Distribution with Log-Normal Fit for MRP-55 Alloy 600 Data

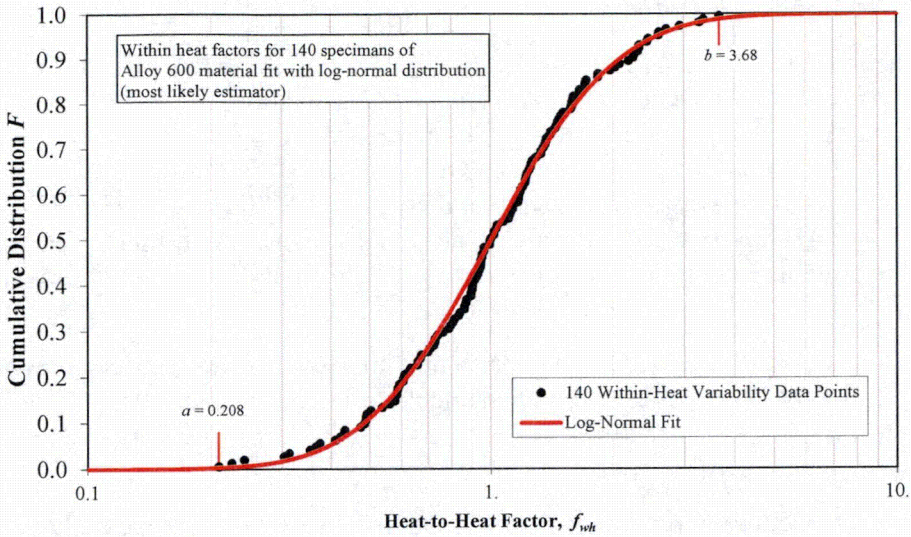

Figure B-24
Within-Heat Factor f_{wh} Distribution with Log-Normal Fit for MRP-55 Alloy 600 Data

B.8.4 Flaw Inspection and Detection Model

The set of inputs for the flaw examination models is described in Table B-9 at the end of this section, including deterministic and distributed inputs. Various inputs are detailed in the following subsections.

B.8.4.1 Examination Scheduling

As mentioned in the modeling section, UT inspection scheduling prior to peening for RPVHPNs is based on N-729-1 [4]. In accordance with this standard, a UT inspection is simulated once every cycle for the hot head (605°F operating temperature, 0.97 capacity factor, 24-month operating cycle) and once every three cycles for the cold head (561°F operating temperature, 0.97 capacity factor, 24-month operating cycle). The first UT inspection is modeled as occurring at the end of the 10th cycle for both the hot and cold reactor pressure vessel heads. These cycles correspond with the specific units that were used to develop the operating timeline, temperature, geometry inputs discussed in Section B.8.1.

In accordance with N-729-1, BMV inspections for leakage are conducted once every two cycles while a head has less than 8.0 EDY of operation and once every cycle afterward. This BMV schedule is not permitted to be relaxed after peening for hot heads but is relaxed to every third outage for cold heads (after follow-up examinations are performed).

In cases where peening is scheduled, the follow-up and in-service inspection intervals are varied to generate comparative results. The follow-up interval is varied between 1, 2, 3, or 1 and 2 cycles for hot heads and between 1, 2, and 3 cycles for cold heads. The in-service inspection interval is varied from 3 cycles to the plant operational service period for the hot and cold heads.

B.8.4.2 UT Probability of Detection

The probabilistic UT POD model is described by Equation [B-14]. The model is generated from upper and lower POD curves which each represent a two standard deviation offset from the median POD curve. The upper bound (favorable) curve was chosen such that there is an 80% POD for cracks 20% through-wall and a 95% POD for cracks 40% through-wall. The lower bound (unfavorable) curve was chosen such that there is a 65% POD for cracks 40% through-wall and a 90% POD for cracks 70% through-wall. Finally, a maximum POD of 95% is used to account for human/equipment error or other factors. The median POD curve is shown in Figure B-25.

This UT POD curve was calibrated to be consistent with a lower-end flaw detection rate for qualification testing of UT procedures and personnel used to inspect RPVHPNs. These UT qualification testing requirements are defined in 10 CFR 50.55a(g)(6)(ii)(D)(*4*) and in Table VIII-S10-1 of Supplement 10 to Appendix VIII of Section XI.

A correlation coefficient relating the results of successive inspections can be included to take into account the increasing likelihood of non-detection if a crack has already been missed in a previous inspection. Because this value has not been experimentally determined, a modest correlation coefficient of 0.5 is used for the base case input.

B.8.4.3 BMV Probability of Detection

The BMV inspection model employs a constant POD, irrespective of leak rate, duration of leak, etc. A value of 90% is used as a conservative assumption based on plant experience that through-wall cracking of CRDM and CEDM nozzles is accompanied by boric acid deposits that are reliably detected during direct visual examinations of the intersection of the nozzle with the upper surface of the reactor vessel head [13].

A strong correlation coefficient, 0.95, is used to correlate successive inspections of the same leaking penetration. It can be shown numerically that this results in approximately a 21%, 17%, and 14% POD for a leaking nozzle at the first, second, and third inspections following an original inspection in which a leaking nozzle was not detected.

Table B-9
Summary of Inputs for RPVHPN Examination Model

Symbol	Description	Source	Units	Parameter Type	Hot Head Base Case	Cold Head Base Case
	The through-wall fraction below which the small-flaw contingency (POD = 0) is used	Smallest flaw size used in UT mockup testing	-		0.10	0.10
$\rho_{insp,UT}$	Correlation coefficient for successive UT inspections	Conservative assumption	-		0.50	0.50
$(a/t_{U,1,UT}, p_{U,1,UT})$	First defined coordinate for favorable UT POD curve	Conservative assumption relative to UT qualification criteria	-		(0.2,0.80)	(0.2,0.80)
$(a/t_{U,2,UT}, p_{U,2,UT})$	Second defined coordinate for favorable UT POD curve	Conservative assumption relative to UT qualification criteria	-		(0.4,0.95)	(0.4,0.95)
$(a/t_{L,1,UT}, p_{L,1,UT})$	First defined coordinate for unfavorable UT POD curve	Conservative assumption relative to UT qualification criteria	-		(0.4,0.65)	(0.4,0.65)
$(a/t_{L,2,UT}, p_{L,2,UT})$	Second defined coordinate for unfavorable UT POD curve	Conservative assumption relative to UT qualification criteria	-		(0.7,0.90)	(0.7,0.90)
	Stdev between median UT POD curve and favorable/unfavorable curves	Conservative assumption relative to UT qualification criteria	-		2	2
$p_{max,UT}$	Maximum probability of detection for UT inspection	Conservative assumption relative to UT qualification criteria	-		0.95	0.95
p_{BMV}	Probability of detection for visual inspection of leaking nozzle	Conservative assumption	-		0.90	0.90
$\rho_{insp,BMV}$	Correlation coefficient for successive BMV inspections	Conservative assumption	-		0.95	0.95

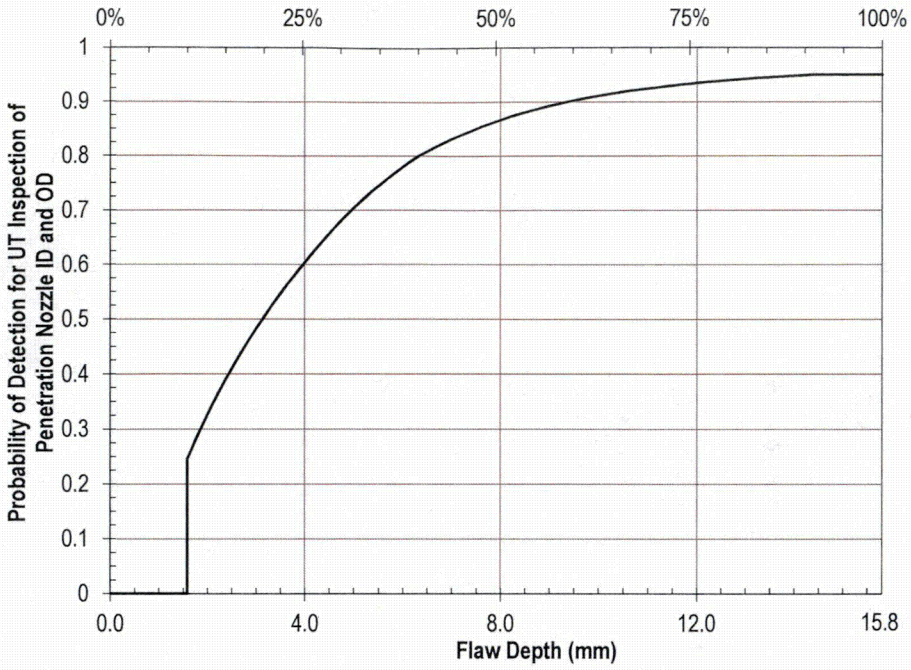

Figure B-25
Median Assumed UT Inspection POD Curve for Axial Cracking Initiating at the RPVHPN ID and OD

B.8.5 Effect of Peening on Residual Stress

The set of inputs related to peening considerations is described in Table B-10 at the end of this section, including deterministic and distributed inputs. Various inputs are detailed in the following subsections.

B.8.5.1 Peening Application Scheduling

The peening applications for the hot and cold head are scheduled based on the operating and inspection experience of the subpopulation of reactor vessel heads with Alloy 600 penetration nozzles that are still in service in U.S. PWRs. Peening application is considered to occur during a cycle that coincides with a scheduled UT inspection.

The hot head has peening scheduled at EOC 17 resulting in 7 UT inspections prior to peening (not including the pre-inspection).

The cold head has peening scheduled at EOC 12 resulting in 1 UT inspection prior to peening (not including the pre-inspection).

B.8.5.2 Post-Peening Residual Stresses

For RPVHPNs, the residual plus normal operating stress is modeled to result in a compressive stress prior to applying operating stresses. Once operating stresses are applied, the post-peening surface stress is deterministically modeled to be +10 ksi. This stress bounds the total steady-state surface stress permitted by the performance criteria in Section 4.

The peening compressive residual stress depth for the RPVHPN is modeled with a normal distribution. For the OD and weld surfaces, this distribution is given a mean of 1.0 mm (minimum allowable compressive residual stress depth defined in Section 4) and a standard deviation of 0.25 mm. For the ID surfaces, this distribution is given a mean of 0.25 mm (minimum allowable compressive residual stress depth defined in Section 4) and a standard deviation of 0.06 mm.

Finally, the same transition length ratios defined in Section A.8.5.2 are applied for peening stress profiles on RPVHPNs.

B.8.5.3 Effect of Thermal and Load Cycling

The peening performance requirements of Section 4 require the compressive stress effect produced by the mitigation process to be effective for at least the remaining service life of the component. As a bounding peening stress profile is applied to this analysis for the remainder of the plant operational period, relaxation effects are not modeled for the RPVHPN base case or for any model sensitivity studies.

B.8.5.4 Effect of Peening on Growth

For base case results, growth of cracks is simulated without consideration for crack closure. This effect is considered as a sensitivity case.

Also for the baseline results, full credit is given to growth of the length of a crack under the peening surface. As discussed in the modeling section, this is done by using the "balloon" growth approximation—neglecting peening stresses for the calculation of length growth. The "balloon" growth approximation is lifted for a sensitivity study.

B.8.6 Flaw Stability Model

The two key inputs to the flaw stability model presented in this report are the initial size of a circumferential through-wall crack and the critical crack length at which ejection is predicted to occur. Both are deterministic inputs and are presented in Table B-11.

Via the conservative precedent set in MRP-105 [5], circumferential through-wall cracks along the weld contour are assumed to initiate with a length equivalent to 30° around the weld contour. Together with the immediate transition to through-wall growth on the weld contour after leakage and accelerated growth parameters, this results in conservative estimates for the time to ejection following leakage.

The critical crack length for ejection, or net section collapse, is based on calculations presented in MRP-110 (Appendix D of Reference [13]). A length equivalent to 300° around the weld contour is used for all base case analyses in this report in order to bound the critical flaw angles calculated for CRDM and CEDM nozzles for all U.S. PWRs under standard design pressure. (For a sensitivity case presented later, the critical flaw length of 275° is used based on MRP-110 calculations in which a structural factor of 2.7 was applied to the standard design pressure.)

Table B-10
Summary of Peening-Specific Inputs

Symbol	Description	Source	Units	Parameter Type	Hot Head Base Case	Cold Head Base Case
	Outage of peening application	Scheduled at next outage coinciding with a UT inspection	Cycle number		17	12
	Number of cycles between peening application and final follow-up inspection	Section 4	# cycles		2	2
	Inspection interval after peening	Section 4	# cycles		5	5
	Interval for BMV post-peening (in number of cycles)	Section 4	# cycles		0	3
	Flag indicating if a UT pre-peening exam is performed	Section 4	-		TRUE	TRUE
	Flag indicating if a UT exam is included during all the cycle(s) between peening and the follow up exam	Section 4	-		TRUE	FALSE
	Flag indicating if BMV exams are performed after peening	Section 4	-		TRUE	TRUE
	Number of consecutive cycles in which BMV exams are performed after peening	Section 4	# cycles		Perform BMV post-peening per Section 4	2

Table B-10 (continued)
Summary of Peening-Specific Inputs

Symbol	Description	Source	Units	Parameter Type	Hot Head Base Case	Cold Head Base Case
$\sigma_{0,PPRS,ID}$ ($t=0$)	Sum of post-peening residual plus normal operating stress on ID surface	Bounds minimum value from performance criteria (Section 4)	ksi		10.0	10.0
$x_{1,PPRS,ID}$	Depth of compressive residual stress layer from ID surface	Bounds minimum value from performance criteria (Section 4)	in.	type	Normal	Normal
				mean	0.010	0.010
				stdev	0.002	0.002
				min	0.000	0.000
				max	0.025	0.025
$\sigma_{0,PPRS,ext}$ ($t=0$)	Sum of post-peening residual plus normal operating stress on OD and weld surface	Bounds minimum value from performance criteria (Section 4)	ksi	mean	10.0	10.0
$x_{1,PPRS,ext}$	Depth of compressive residual stress layer from OD and weld surface	Bounds minimum value from performance criteria (Section 4)	in.	type	Normal	Normal
				mean	0.039	0.039
				stdev	0.010	0.010
				min	0.000	0.000
				max	0.098	0.098
$f_{1,PPRS}$	Ratio of minimally-affected depth to penetration depth	Section A.3.3	-		2.0	2.0
$f_{2,PPRS}$	Fraction of depth between penetration depth and minimally-affected depth where peening results in no effect	Section A.3.3	-		0.7	0.7

Table B-11
Summary of Inputs for RPVHPN Stability Model

Symbol	Description	Source	Units	Parameter Type	Hot Head Base Case	Cold Head Base Case
$\theta_{circ,init}$	Initial angle for circumferential through-wall cracks immediately following a leak	MRP-105	degrees		30	30
$\theta_{circ,crit}$	Critical flaw angle for nozzle ejection	MRP-110	degrees		300	300
$K_{circ,mult}$	Circumferential through-wall crack K_I curve multiplier	Assumed to assure conservative application of FEA-predicted K_I curves	-	type	triangular	triangular
				mode	1	1
				lower limit	1	1
				upper limit	2	2
$c_{circ,mult}$	Circumferential through-wall crack environmental factor	Conservative factor applied based on anecdotal information about environment effects on circumferential TW cracks	-	type	triangular	triangular
				mode	1	1
				lower limit	1	1
				upper limit	2	2

B.9 Results of Probabilistic Cases

This section presents results generated using the integrated probabilistic model described in Sections B.2 through B.6, with particular focus on the prediction of the ejection criterion described in Section B.7. Using the inputs described in Section B.8, this section presents predictions for PWSCC on RPVHPNs on a hot and cold head, without peening mitigation (Section B.9.1) and with peening mitigation (Section B.9.2).

Section B.9.3 presents the results of sensitivity studies wherein one or more inputs or modeling methodologies are varied from those described in Sections B.2 through B.8. The aim of these sensitivity studies is to demonstrate the relative change in the predicted ejection risk for a head when an input or modeling assumption is varied.

Ejections and leakage are counted in two different ways within the simulation framework: in terms of the number of heads with at least one event (by counting only the first instance of leakage or ejection for a given MC realization) and in terms of the number of penetrations with at least one event (by counting the first instance of leakage or the occurrence of ejection for each unique penetration). The primary ejection and leakage statistics used to assess and compare the results of the probabilistic model are defined below:

- Incremental leakage frequency (ILF) is defined as the average number of new leaking nozzles per year on a reactor vessel top head. A simulated flaw causes leakage if it propagates through the entire material thickness to penetrate the annulus above the J-groove weld before it is detected and repaired. This statistic is derived for any given operational cycle by averaging the predicted number of new leaking nozzles for that operational cycle across all MC realizations. This is adjusted to a probability per year by dividing by the number of calendar years per cycle.

$$ILF = \frac{(\text{Number of new leaking nozzles predicted during cycle across all realizations})}{(\text{Number of realizations})(\text{Calendar years per cycle})} \qquad \text{[B-16]}$$

- Average leakage frequency (ALF) is the average of the ILFs following the hypothetical time of peening until the end of the operational service period of the plant.

$$ALF = \frac{\sum_{i=i_{peen}}^{N_{cycle}} (\text{Number of new leaking nozzles predicted during cycle across all realizations})}{(\text{Number of realizations})(\text{Calendar years per cycle})(N_{cycle} - i_{peen})} \qquad \text{[B-17]}$$

where:

N_{cycle} = number of cycles in operational service period
i_{peen} = cycle number associated with the hypothetical time of peening

- Cumulative probability of leakage (CPL) is defined as the fraction of heads with at least one predicted leak across all MC realizations across all cycles of interest. This document reports two versions of this statistic: (1) cumulated from the start of operation to a given cycle and (2) cumulated from the hypothetical time of peening to the end of plant operation.

$$CPL = \frac{\text{(Total number of heads with at least one predicted leak)}}{\text{(Number of realizations)}} \quad \text{[B-18]}$$

- Incremental ejection frequency (IEF) is defined as the average number of nozzle ejections per year on a reactor vessel top head. This statistic is derived for any given operational cycle by averaging the predicted number of ejections for that operational cycle across all MC realizations and dividing by the number of calendar years per cycle. If no ejections are predicted to occur during a given cycle across all MC realizations, 0.5 ejections are assumed for the sake of stability and conservatism in calculated statistic values.

$$IEF = \frac{\max\{\text{(Number of ejections leaks predicted during cycle across all realizations)},0.5\}}{\text{(Number of realizations)(Calendar years per cycle)}} \quad \text{[B-19]}$$

- Average ejection frequency (AEF) is the average of the IEFs following the hypothetical time of peening until the end of the operational service period of the plant.

$$AEF = \frac{\sum_{i=i_{peen}}^{N_{cycle}} \max\{\text{(Number of ejections predicted during } i\text{th cycle across all realizations)},0.5\}}{\text{(Number of realizations)(Calendar years per cycle)}(N_{cycle} - i_{peen})} \quad \text{[B-20]}$$

- Cumulative probability of ejection (CPE) is defined as the fraction of heads with at least one predicted ejection across all MC realizations across all cycles of interest. This document reports two versions of this statistic: (1) cumulated from the start of operation to a given cycle and (2) cumulated from the hypothetical time of peening to the end of plant operation.

$$CPE = \frac{\text{(Total number of heads with at least one predicted ejection)}}{\text{(Number of realizations)}} \quad \text{[B-21]}$$

The effect of nozzle ejection on nuclear safety can be assessed through multiplication of the frequency of nozzle ejection (i.e., the initiating event frequency) with appropriate conditional core damage probability (CCDP) value. The resulting core damage frequency is typically averaged over long-term operation and compared to the acceptance criteria of Regulatory Guide 1.174 [15]. Regulatory Guide 1.174 specifies an acceptable change in core damage frequency of 1×10^{-6} per reactor year for permanent changes in plant design parameters, technical specifications, etc.

In addition to comparison versus the absolute acceptance criterion of Regulatory Guide 1.174, the results of the probabilistic modeling can be used to make relative comparisons of the statistics predicted for different cases (e.g., between the AEF predicted for one peening schedule vs. the AEF predicted for the unmitigated case with standard inspection intervals). This comparative approach has the advantage of minimizing any potential for bias introduced by the various modeling assumptions.

B.9.1 Results for the Unmitigated Case

Using the inputs specified in Section A.8, predictions were made for unmitigated RPVHPNs. Ejection predictions for hot and cold heads are shown in Figure B-26 and Figure B-27, leakage

predictions are shown in Figure B-28 and Figure B-29. For these results, volumetric and visual examinations were scheduled based on N-729-1 for unmitigated reactor vessel heads.

For reference, the time of the first modeled inspection, as well as the hypothetical time of peening is shown on these plots. Between the hypothetical time of peening and 60 calendar years (58.2 EFPY), the model predicts an average ejection frequency (AEF) of 2.1×10^{-5} for the hot head and 1.9×10^{-6} for the cold head; the model predicts a cumulative probability of leakage of 18.6% for the hot head and 18.4% for the cold head.

These values will be important for assessing the performance of peening for leakage mitigation in the following section.

B.9.2 Results with Peening Mitigation

As discussed previously, a follow-up inspection is expected to be conducted either one, two, three, or the first and second cycles after peening for the hot head, and either one, two, or three cycles after peening for the cold head. After the follow-up inspection, a new in-service inspection interval is expected to be utilized through the end of plant service life. Various combinations of follow-up inspection time and in-service inspection frequency were used to make ejection and leakage predictions after peening. Ejection results are summarized in Figure B-30 for the hot head case and in Figure B-31 for the cold head case, and leakage results are summarized in Figure B-32 and Figure B-33 for the hot and cold head cases, respectively.

The RPVHPN results demonstrated a much larger trend with respect to the ISI frequency than the DM weld results. This is due in large part to the higher likelihood of cracks existing after the pre-peening inspection. It is conservatively predicted that, on average, two nozzles in each hot head and one nozzle in approximately two cold heads would have unrepaired cracks after the pre-peening inspection.

For both the hot and cold heads, the cumulative probability of leakage after peening is predicted to be reduced by a factor between 3.5 and 6 times, depending on the post-peening inspection schedule. For example, using a 10-year (one interval) UT inspection frequency, the cumulative probability of leakage after peening is predicted to be reduced by a factor of approximately five for both hot and cold heads. Furthermore, the probability of leakage vs. time decays rapidly for both hot and cold heads with relieve UT inspection intervals, as shown in Figure B-34.

For the hot head reactor, using a post-peening ISI interval of 10 years (one interval) combined with a follow-up examination either one or two cycles after peening resulted in somewhat higher ejection risks than the unmitigated case: 182% and 147% of the unmitigated head risk, respectively. However, the same interval with a follow-up inspection both one and two cycles after peening resulted in an ejection risk lower than (83% of) the unmitigated case.

For the cold head reactor, the AEF after peening was predicted to improve compared to the unmitigated case when a post-peening ISI frequency of every 10 years (one interval) is used with a follow-up within 6 calendar years after peening. A post-peening ISI of one interval resulted in somewhat lower ejection risks compared to the unmitigated case: 79%, 45%, and 66% of the unmitigated risk for follow-up inspections scheduled one, two, and three cycles after peening, respectively. This result suggests that it may be beneficial to delay the follow-up inspection to the second cycle after peening to allow more significant cracks to grow such that they are more easily detected at the follow-up inspection, i.e., before entering the ISI schedule.

It is important to consider the maximum incremental frequency of ejection (IEF) for any cycle, in addition to the AEF, in order to understand how concentrated the risk may be over particular spans of time and if there are particular cycles with considerably higher risk. For instance, for the peened cold head base case (with a follow-up inspection two cycles after peening and an ISI interval of 5 cycles), the ratio of maximum IEF to AEF is 4.0. The same ratio for the unmitigated cold head is 3.60. For a peened hot head (with a follow-up inspection one and two cycles after peening and an ISI interval of 5 cycles), the ratio of maximum IEF to AEF was 3.1. The same ratio for the unmitigated hot head is 1.4. The risk concentration was not substantially worse for the peened case than for the unmitigated case.

Comparing the leakage and ejection statistics recorded for the head as a whole and the statistics recorded for individual nozzles, it is possible to draw conclusions regarding the number of incidences per head *assuming that the head has one or more of such incidences (assuming one or more leaks or one or more ejections)*. For instance, hot heads that are predicted to have no ejections or repairs prior to the outage before peening are anticipated to have approximately 1.1 leaking penetrations between peening and the end of service; hot heads that are predicted to have no ejections or repairs prior to the outage before peening are anticipated to have only one ejection by the end of service (under the assumption that a unit would continue operating without head replacement after the first ejection). However, it is important to keep in mind that the average ejection frequency is four orders of magnitude lower than the average leakage frequency.

Finally, some location-specific information is output by the RPVHPN program. This information indicates that as modeled 75% to 90% or more of leaks that occur after peening occur due to weld-initiated cracks. The leakage probability as calculated is greatly influenced by the conservative assumptions that one third of the crack initiations occur on the wetted surface of the weld metal and that the weld flaws grow to cause leakage with no chance of becoming detectable via UT performed from the nozzle inside surface. On the contrary, plant experience shows that most CRDM nozzles leaks have been accompanied by cracking of the nozzle tube base metal detectable via UT from the nozzle inside surface. The assumptions made in the modeling conservatively increase the chance of developing circumferential cracks in the nozzle tube above the weld elevation since a 30° through-wall circumferential crack is assumed to be produced immediately upon leakage. The probability of leakage due to base metal cracking is also a more relevant measure to assess the benefit of periodic UT examinations because such examinations are not qualified to detect weld flaws.

B.9.3 Results for Sensitivity Cases

Various sensitivity studies were conducted with the RPVHPN probabilistic model in order to demonstrate the relative change in the predicted results given one or more changes to modeling or input assumptions. Each sensitivity case has been classified as either a Model Sensitivity Case (in which an approximated input or model characteristic is varied) or an Inspection Scheduling Sensitivity Case (in which a controllable inspection option is varied). Modified inputs for Model Sensitivity Cases are presented in Table B-12, modified inputs for Inspection Scheduling Sensitivity Cases are presented in Table B-13.

For hot heads, Figure B-35 compares the average ejection frequencies from the peening inspection scheduling sensitivity cases to those for the peening and non-peening base cases.

Figure B-36 and Figure B-37 compare the AEFs resulting from the model sensitivity cases with peening to those for the peening base case. Figure B-38 and Figure B-39 compare the AEFs resulting from the model sensitivity cases with no-peening to those for the no-peening base case.

For cold heads, Figure B-40 compares the average ejection frequencies from the peening inspection scheduling sensitivity cases to those for the peening and non-peening base cases. Figure B-41 compares the AEFs resulting from the model sensitivity cases with peening to those for the peening base case. Figure B-42 compare the AEFs resulting from the model sensitivity cases with no-peening to those for the no-peening base case.

The cases of greatest interest are discussed below:

Inspection Scheduling Sensitivity Case 1 – Entering Post-Peening ISI without a Follow-Up Inspection & Inspection Scheduling Sensitivity Case 2 – No Pre-Peening Inspection

Inspection Scheduling Sensitivity Case 1 explored that result of skipping the follow-up UT inspection after peening and immediately entering a post-peening ISI with a UT inspection frequency of once every 5 cycles (one interval). Inspection Scheduling Sensitivity Case 2 explored that result of skipping the pre-peening UT inspection but conducting a follow-up UT the first and second cycle after peening before entering a post-peening ISI defined in Section 4. In both cases, BMV inspection was performed according to N-729-1 schedule requirements.

Not performing follow-up inspections (Inspection Scheduling Sensitivity Case 1) resulted in an AEF of 1.0×10^{-4} for the peened hot-head, and an AEF of 2.1×10^{-6} for the peened cold-head. Not performing pre-peening inspections (Inspection Scheduling Sensitivity Case 2) resulted in an AEF of 8.0×10^{-5} for the peened hot-head, and an AEF of 1.9×10^{-6} for the peened cold-head. These sensitivity cases emphasize the importance of both the pre-peening and follow-up examinations.

Inspection Scheduling Sensitivity Case 3 through 5 – Various Relief Options for Post-Peening Visual Examinations

As discussed previously, N-729-1 requires that VE be performed every cycle on unmitigated heads with more than 8.0 EDY. Inspection Scheduling Sensitivity Cases 3 through 5 explored the use of a different BMV schedule after peening:

- Case 3 used a two-cycle BMV interval after peening.
- Case 4 used a three-cycle BMV interval after peening.
- Case 5 stopped BMV examinations altogether after peening.

Figure B-35 and Figure B-40 demonstrate the effect of each BMV scheduling change, relative to the base case.

The use of a two-cycle BMV interval after peening resulted in an AEF of 3.1×10^{-5} for the peened hot head, and an AEF of 1.1×10^{-6} for the peened cold head. Moving to a three-cycle BMV resulted in an AEF of 4.3×10^{-5} for the peened hot head. Not performing BMV altogether after peening resulted in an AEF of 2.4×10^{-4} for the peened hot head, and an AEF of 7.5×10^{-6} for the peened cold head, demonstrating the value in performing periodic BMV examinations. It is noted that these probabilistic results do not credit the performance of required IWA-2212 VT-2 visual

examinations of the head under the insulation through multiple access points every outage that a VE is not performed.

Model Sensitivity Case 2 –Reactor Vessel Heads with No Observed PWSCC to Date

Model Sensitivity Case 2 explored the result of resampling Monte Carlo realizations in which crack detection or nozzle ejection was predicted prior to the outage before that in which peening occurs.

This resampling logic results in probabilities that are conditioned on the premise that no detection of PWSCC or ejection has taken place by the specified time; of the 5 active hot heads and 19 active cold heads with Alloy 600 nozzles in U.S. PWRs, PWSCC has been reported for only six heads to date (one of which was a hot head) despite multiple volumetric examination having been performed of all the nozzles in each head [3].

Resampling early detections or ejections results in an AEF of 2.8×10^{-6} for the peened hot head, an AEF of 3.0×10^{-6} for the unmitigated hot head, an AEF of 5.3×10^{-7} for the peened cold head, and an AEF of 6.3×10^{-7} for the unmitigated cold head. Approximately three of every four Monte Carlo realizations are resampled for the hot head, and about one in 10 realizations are resampled for the cold head.

Figure B-43 shows a time-history of the incremental ejection frequency and cumulative probabilities of ejection for this sensitivity case. By comparing these results to the base case results shown in Figure B-26, it is clear that resampling MC realizations that are conditioned on no early detection or ejections results in a lower IEF and CPE. Comparing this sensitivity case to the equivalent peening or unmitigated base case, the average ejection frequency is about a factor of 6.2 lower for the peened hot head, a factor of 6.9 lower for the unmitigated hot head, a factor of 2.4 lower for the peened cold head, and a factor of 3.1 lower than the base case for the unmitigated cold head.

Model Sensitivity Cases 7 and 9 – Removal of Inspection Correlation

As discussed in the modeling and inputs section, the base case assumed correlation between successive inspections, i.e., a crack that goes undetected by a UT examination would be more likely to be missed in subsequent UT inspections (assuming it does not grow significantly); a leak that goes undetected by visual examination is more likely to be missed in subsequent visual examinations.

Removing correlation between subsequent UT inspections (M7) results in an AEF of 1.1×10^{-5} for the peened hot head, and an AEF of 1.6×10^{-5} for the unmitigated hot head. Removing correlation between subsequent BMV inspections (M9) results in an AEF of 3.3×10^{-6} for the peened hot head, an AEF of 1.6×10^{-5} for the unmitigated hot head, an AEF of 5.6×10^{-7} for the peened cold head, and an AEF of 9.9×10^{-7} for the unmitigated cold head.

The inclusion of these correlations results in higher probabilities of leakage and ejection because it reduces the benefit of performing multiple examinations over time to detect a crack or leak, allowing longer spans of time for growth.

Model Sensitivity Case 13 – Earlier Initiation of First PWSCC

Similar to DMW Model Sensitivity Case 13, this case explored the shifting of the initiation time model to earlier times. For this sensitivity case, t_1, the time at which 1% of all RPVHPNs are expected to initiate PWSCC, was reduced by a factor of 5.

This shift in the initiation model resulted in an AEF of 3.3×10^{-5} for the peened hot head, an AEF of 2.9×10^{-5} for the unmitigated hot head, an AEF of 8.3×10^{-6} for the peened cold head, and an AEF of 1.0×10^{-5} for the unmitigated cold head. The predicted AEF and ALF for this sensitivity case result in the greatest increase with respect to the base case. However, it is noted that this initiation model results in a prediction of at least one leaking nozzle before 20 EFPY in over 95% of hot-heads and in over 35% of cold-heads. This is not in line with U.S. PWR operating experience.

Model Sensitivity Case 16 – Correlation Between Initiation and Growth

Similar to DMW Model Sensitivity Case 15, this case explored the generally accepted tendency for cracks that initiate earlier to grow faster.

Including this correlation results in an AEF of 1.7×10^{-5} for the peened hot-head, an AEF of 3.7×10^{-5} for the unmitigated hot-head, an AEF of 4.1×10^{-6} for the peened cold-head, and an AEF of 1.0×10^{-5} for the unmitigated cold-head.

This significant increase for cold-heads is due to the fact that any instance of PWSCC that initiates prior to the end of the unit operating lifetime are relatively early given the initiation frequency at temperatures characteristic of a cold head. The growth rates of these cracks could be biased upward of laboratory crack growth rate predictions (assuming that the conditions that led to early initiation also foster more rapid growth).

Table B-12
Summary of Modified Inputs for RPVHPN Model Sensitivity Cases

Sensitivity Case	Description	Symbol	Units	Parameter Type	Hot Base Case Value	Hot Sensitivity Case Value	Cold Base Case Value	Cold Sensitivity Case Value
M1	Reduce operating capacity factor	CF	-		0.97	0.92		
M2	Reject trials with detections/ejections before given cycle (i.e. present day)		Cycle number		0	16	0	11
M3	Increase number of modeled penetrations	N_{pen}	-		78	97		
M4	Decrease nozzle thickness and OD	t	in.		0.62	0.39		
		D_o	in.		4.00	3.50		
M5	Halve growth integration time step	$1/\Delta t$	1/yr		12	24		
M6	Linearly extrapolate POD to zero below 10% TW		-		Assume POD = 0 below 10% TW	Linearly extrapolate		
M7	Remove correlation between UT inspections	$\rho_{insp,UT}$	-		0.50	0.00		
M8	Decrease maximum UT probability of detection to 90%	$p_{max,UT}$	-		0.95	0.90	0.95	0.90
M9	Remove correlation between BMV inspections	$\rho_{insp,BMV}$	-		0.95	0.00	0.95	0.00
M10	Decrease critical flaw angle for nozzle ejection	$\theta_{circ,crit}$	degrees		300	275	300	275

Table B-12 (continued)
Summary of Modified Inputs for RPVHPN Model Sensitivity Cases

Sensitivity Case	Description	Symbol	Units	Parameter Type	Hot Base Case Value	Hot Sensitivity Case Value	Cold Base Case Value	Cold Sensitivity Case Value
M11	Double standard deviation of peening penetration depth	$x_{1,PPRS,ID}$	in.	type	Normal	Normal		
				mean	0.010	0.010		
				stdev	0.002	0.005		
				min	0.000	0.000		
				max	0.025	0.049		
		$x_{1,PPRS,ext}$	in.	type	Normal	Normal		
				mean	0.039	0.039		
				stdev	0.010	0.020		
				min	0.000	0.000		
				max	0.098	0.236		
M12	Increase peening compressive surface stress and penetration depth	$\sigma_{0,PPRS,ID}$ (t=0)	ksi		Normal operating plus residual stress is +10 ksi tensile	Residual stress is 100 ksi compressive		
		$x_{1,PPRS,ID}$	in.	type	Normal	Normal		
				mean	0.010	0.020		
				stdev	0.002	0.005		
				min	0.000	0.000		
				max	0.025	0.049		
		$\sigma_{0,PPRS,ext}$ (t=0)	ksi		Normal operating plus residual stress is +10 ksi tensile	Residual stress is 100 ksi compressive		
		$x_{1,PPRS,ext}$	in.	type	Normal	Normal		
				mean	0.039	0.118		
				stdev	0.010	0.059		
				min	0.000	0.000		
				max	0.098	0.295		
M13	Decrease initiation characteristic time by factor of 5	t_1	EDY		23.0	4.6	23.0	4.6
M14	Increase multiple flaw initiation slope	β_{flaw}	-	type	Normal	Normal	Normal	Normal
				mean	2.0	3.0	2.0	3.0
				stdev	0.5	0.5	0.5	0.5
				min	1.0	2.0	1.0	2.0
				max	5.0	6.0	5.0	6.0

Table B-12 (continued)
Summary of Modified Inputs for RPVHPN Model Sensitivity Cases

Sensitivity Case	Description	Symbol	Units	Parameter Type	Hot Base Case Value	Hot Sensitivity Case Value	Cold Base Case Value	Cold Sensitivity Case Value
M15	Sample multiple flaw initiation slope a single time per head		-		Sample multiple flaw initiation slope once per penetration	Sample multiple flaw initiation slope once per head		
M16	Include initiation-growth correlation	ρ_{heat}	-		0.0	-0.8	0.0	-0.8
		ρ_{weld}	-		0.0	-0.8	0.0	-0.8
M17	Decrease initiation activation energy	Q_i	kcal/mole	type			Normal	Normal
				mean			44.03	40.03
				stdev			3.06	3.06
				min			25.65	21.64
				max			62.41	58.41
M18	Decrease median initial crack depth by factor of 5 and remove minimum, impose minimum K_I value	a_0	in.	type	Log-Normal	Log-Normal	Log-Normal	Log-Normal
				linear μ	0.033	0.006	0.033	0.006
				median	0.031	0.006	0.031	0.006
				log-norm μ	-3.467	-5.127	-3.467	-5.127
				log-norm σ	0.354	0.354	0.354	0.354
				min	0.020	0.000	0.020	0.000
				max	0.622	0.622	0.622	0.622
		$K_{I,min,heat}$	ksi-in.$^{0.5}$		0.00	10.92	0.00	10.92
		$K_{I,min,weld}$	ksi-in.$^{0.5}$		0.00	10.92	0.00	10.92
M19	Utilize crack closure methodology and decrease initial flaw depth		-		Do not utilize crack closure	Utilize crack closure	Do not utilize crack closure	Utilize crack closure
		a_0	in.	type	Log-Normal	Log-Normal	Log-Normal	Log-Normal
				linear μ	0.033	0.006	0.033	0.006
				median	0.031	0.006	0.031	0.006
				log-norm μ	-3.467	-5.127	-3.467	-5.127
				log-norm σ	0.354	0.354	0.354	0.354
				min	0.020	0.000	0.020	0.000
				max	0.622	0.622	0.622	0.622
M20	Increase median initial crack depth	a_0	in.	type	Log-Normal	Log-Normal	Log-Normal	Log-Normal
				linear μ	0.033	0.146	0.033	0.146
				median	0.031	0.137	0.031	0.137
				log-norm μ	-3.467	-1.987	-3.467	-1.987
				log-norm σ	0.354	0.354	0.354	0.354
				min	0.020	0.020	0.020	0.020
				max	0.622	0.622	0.622	0.622

Table B-12 (continued)
Summary of Modified Inputs for RPVHPN Model Sensitivity Cases

Sensitivity Case	Description	Symbol	Units	Parameter Type	Hot Base Case Value	Hot Sensitivity Case Value	Cold Base Case Value	Cold Sensitivity Case Value
M21	MRP-55 Crack Growth Rate Model Parameters	α_{heat}	(in/hr)/(ksi-in.$^{0.5}$)$^{1.6}$		3.25E-08	2.21E-07		
		$K_{1,th,heat}$	ksi-in.$^{0.5}$		0.00	8.19		
		n_{heat}	-		1.60	1.16		
M22	Decrease growth activation energy	Q_g	kcal/mole	type			Normal	Normal
				mean			31.07	28.68
				stdev			1.20	1.20
				min			23.90	21.51
				max			38.24	35.85
M23	Prevent balloon growth		-		Allow balloon growth	Prevent balloon growth		
M24	Remove crack environmental factor	$c_{circ,mult}$	-	type	triangular	constant	triangular	constant
				mode	1	1	1	1
				lower limit	1	-	1	-
				upper limit	2	-	2	-
M25	Increase peening compressive surface stress and penetration depth, prevent balloon growth, utilize crack closure	$\sigma_{0,PPRS,ID}$ (t=0)	ksi		Normal operating plus residual stress is +10 ksi tensile	Residual stress is 100 ksi compressive		
		$x_{1,PPRS,ID}$	in.	type	Normal	Normal		
				mean	0.010	0.020		
				stdev	0.002	0.005		
				min	0.000	0.000		
				max	0.025	0.049		
		$\sigma_{0,PPRS,ext}$ (t=0)	ksi		Normal operating plus residual stress is +10 ksi tensile	Residual stress is 100 ksi compressive		
		$x_{1,PPRS,ext}$	in.	type	Normal	Normal		
				mean	0.039	0.118		
				stdev	0.010	0.059		
				min	0.000	0.000		
				max	0.098	0.295		
			-		Do not utilize crack closure	Utilize crack closure		
			-		Allow balloon growth	Prevent balloon growth		

Table B-13
Summary of Modified Inputs for RPVHPN Inspection Scheduling Sensitivity Cases

Sensitivity Case	Description	Symbol	Units	Parameter Type	Hot Base Case Value	Hot Sensitivity Case Value	Cold Base Case Value	Cold Sensitivity Case Value
S1	Skip follow-up UT inspection and enter post peening ISI schedule		-		Perform follow-up UT 1st and 2nd cycle after peening	Skip follow-up UT inspection; first ISI after 5 cycles	Perform follow-up UT 2nd cycle after peening	Skip follow-up UT inspection; first ISI after 5 cycles
S2	Skip UT during pre-peening inspection		-		Perform UT during pre-peening inspection	Skip UT during pre-peening inspection	Perform UT during pre-peening inspection	Skip UT during pre-peening inspection
S3	BMV every other cycle post-peening		-		Perform BMV post-peening per Section 4	Perform BMV every 2nd outage post-peening	Perform BMV post-peening per Section 4	Perform BMV every 2nd outage post-peening
S4	BMV every third cycle post-peening		-		Perform BMV post-peening per Section 4	Perform BMV every 3rd outage post-peening		
S5	Do not perform BMV after peening		-		Perform BMV post-peening per Section 4	Do not perform BMV after peening	Perform BMV post-peening per Section 4	Do not perform BMV after peening
S6	Do not perform UT during all cycles between peening and follow-up exam		-		Perform follow-up UT 1st and 2nd cycle after peening	Perform follow-up UT 2nd cycle after peening		

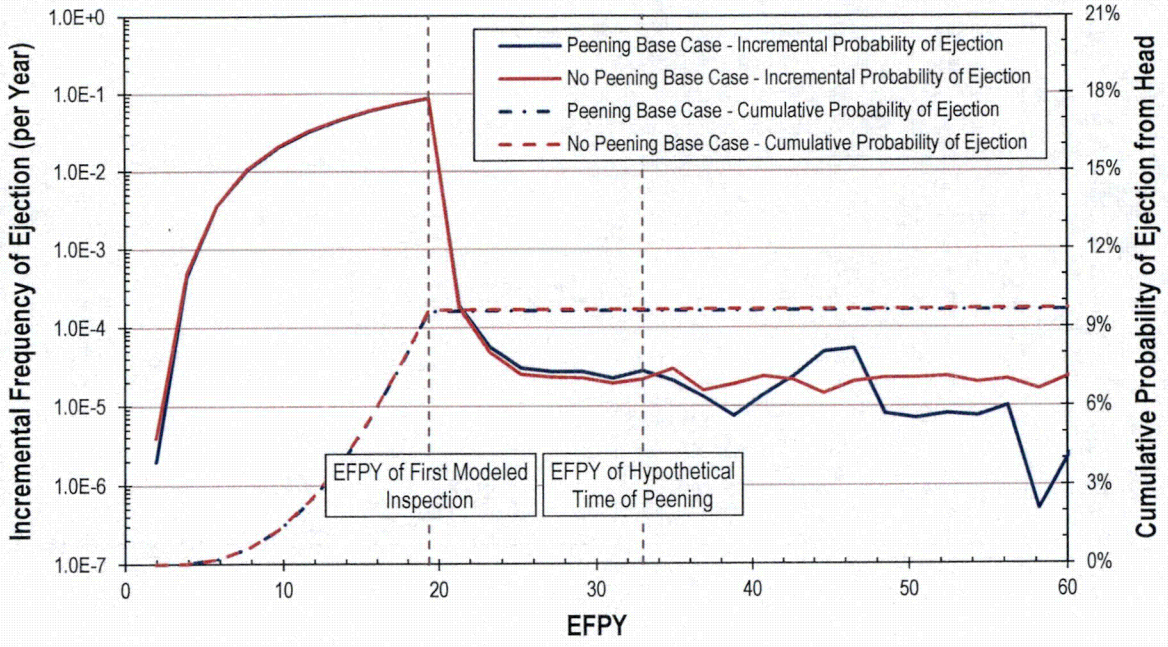

Figure B-26
Prediction of Ejection vs. Time for Hot RPVHPNs

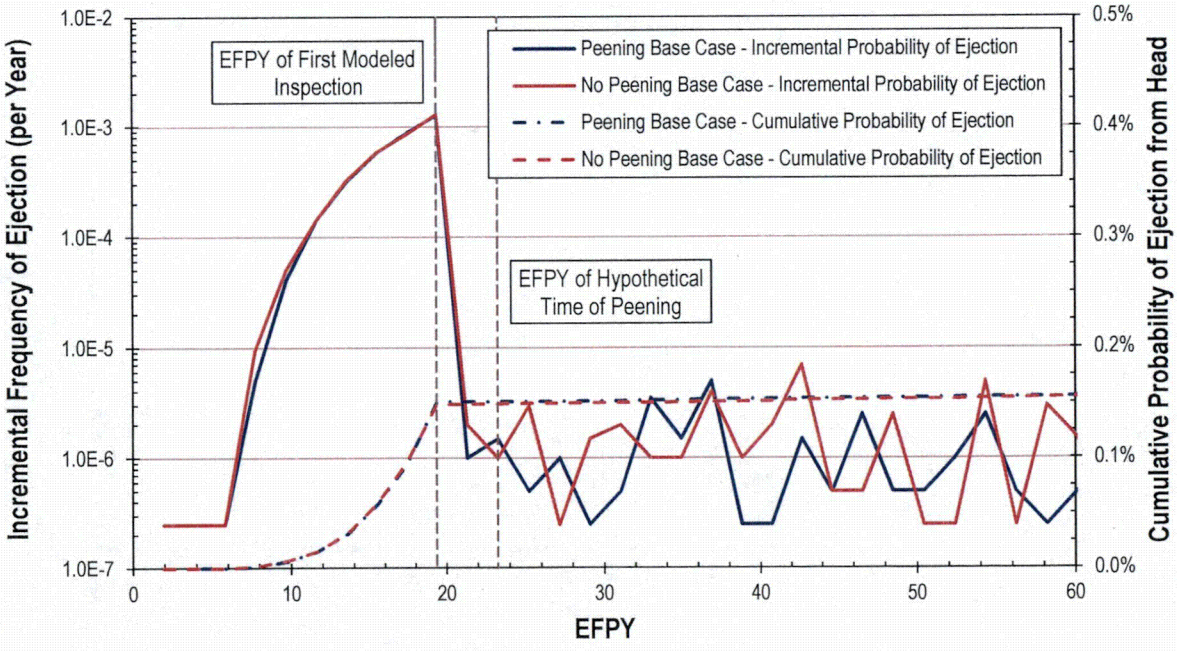

Figure B-27
Prediction of Ejection vs. Time for Cold RPVHPNs

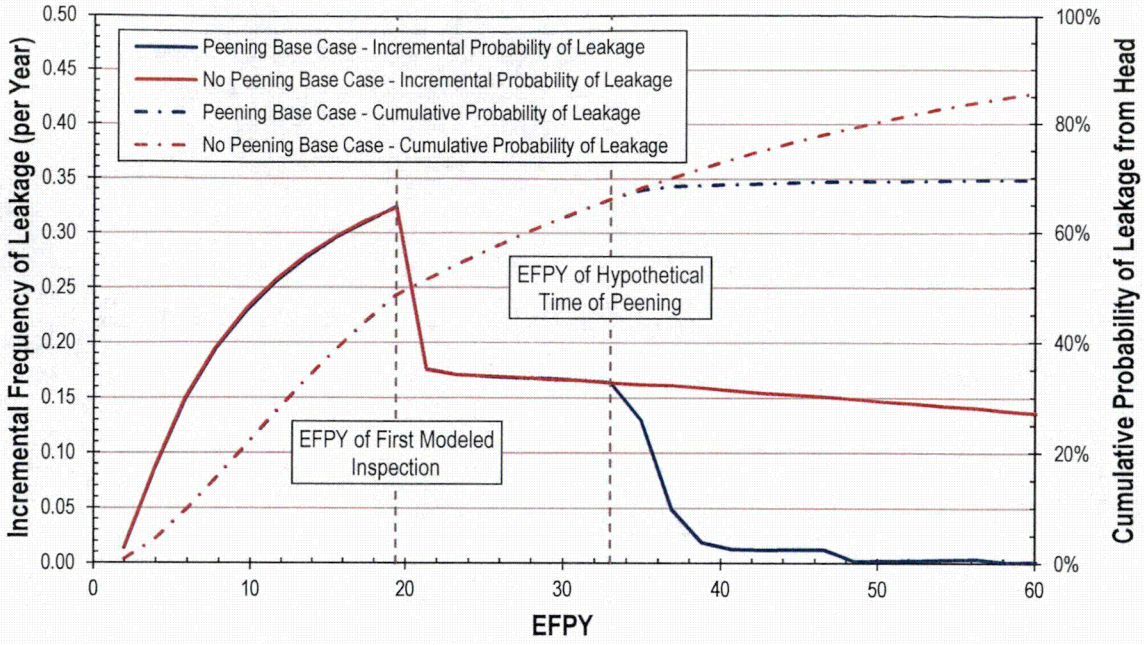

Figure B-28
Prediction of Leakage vs. Time for Hot RPVHPNs

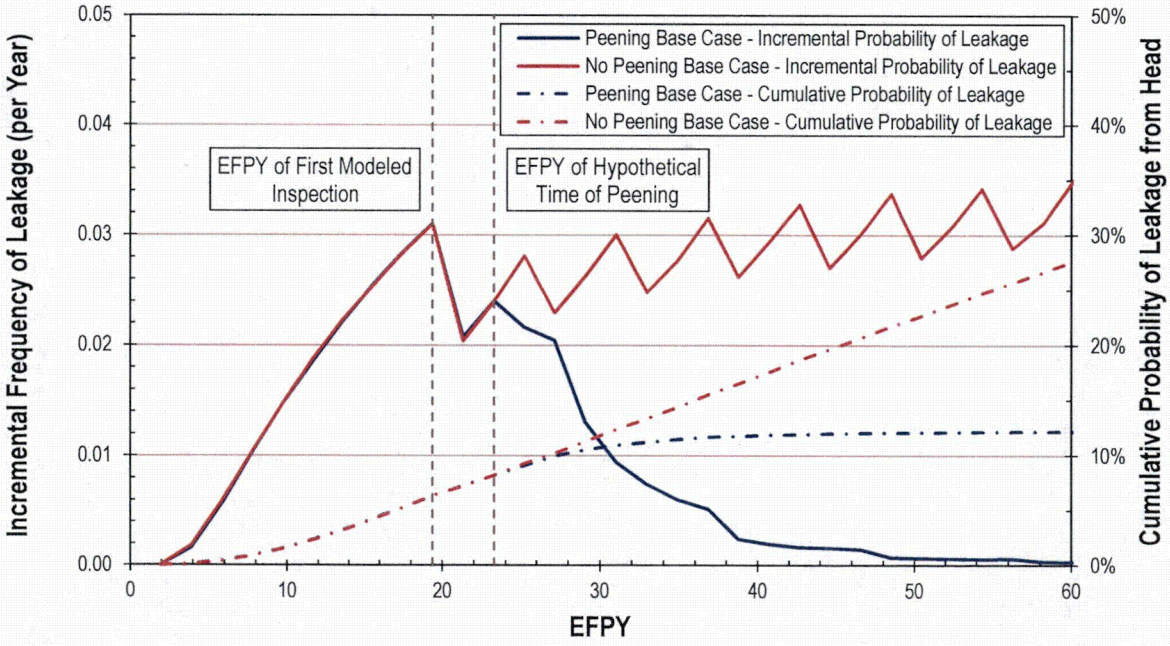

Figure B-29
Prediction of Leakage vs. Time for Cold RPVHPNs

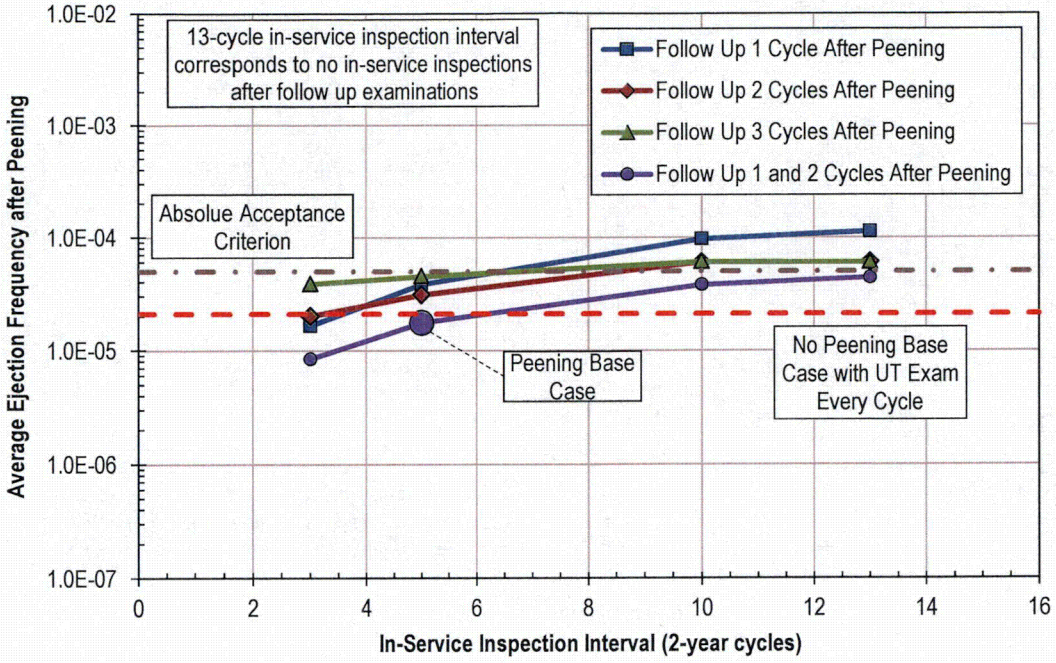

Figure B-30
Average Ejection Frequency from Hypothetical Time of Peening to End of Operational Service Period vs. ISI Frequency for Hot Reactor Vessel Head

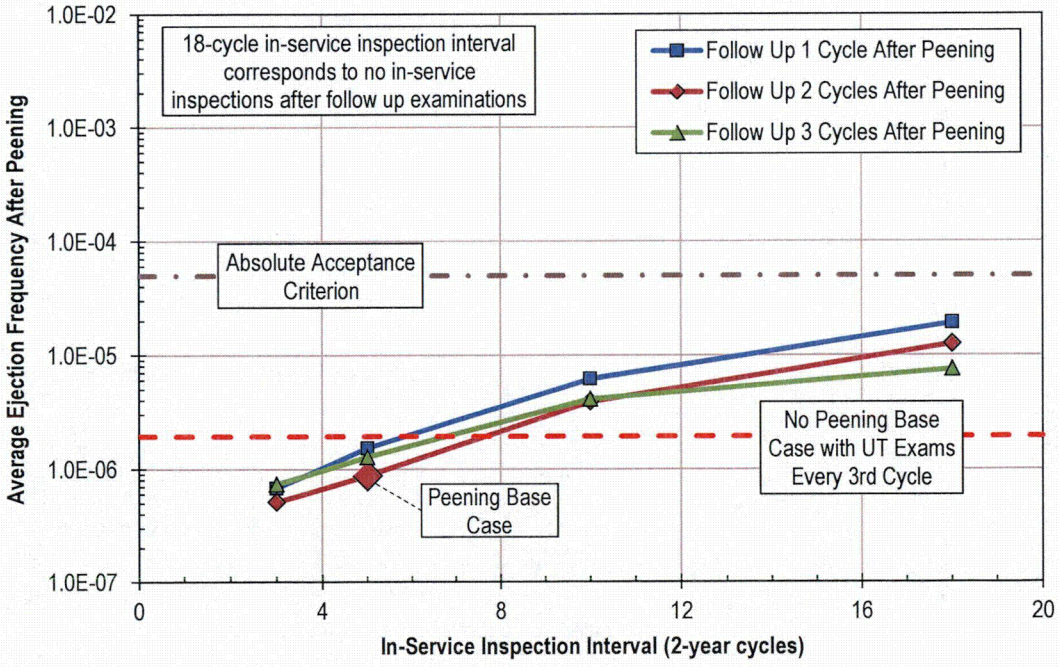

Figure B-31
Average Ejection Frequency from Hypothetical Time of Peening to End of Operational Service vs. ISI Frequency for Cold Reactor Vessel Head

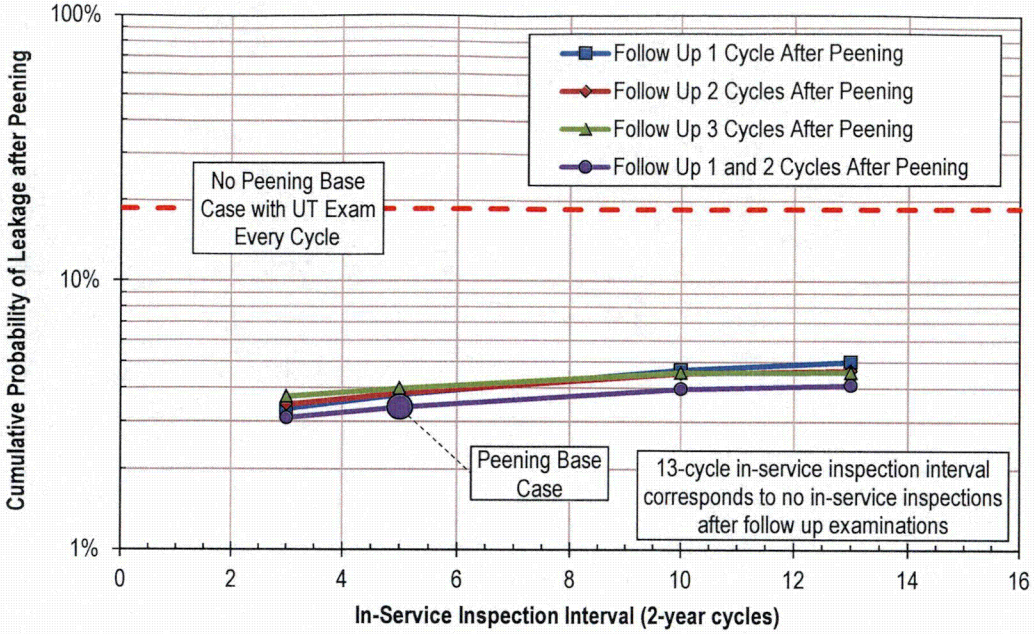

Figure B-32
Cumulative Probability of Leakage from Hypothetical Time of Peening to End of Operational Service Period vs. ISI Frequency for Hot Reactor Vessel Head

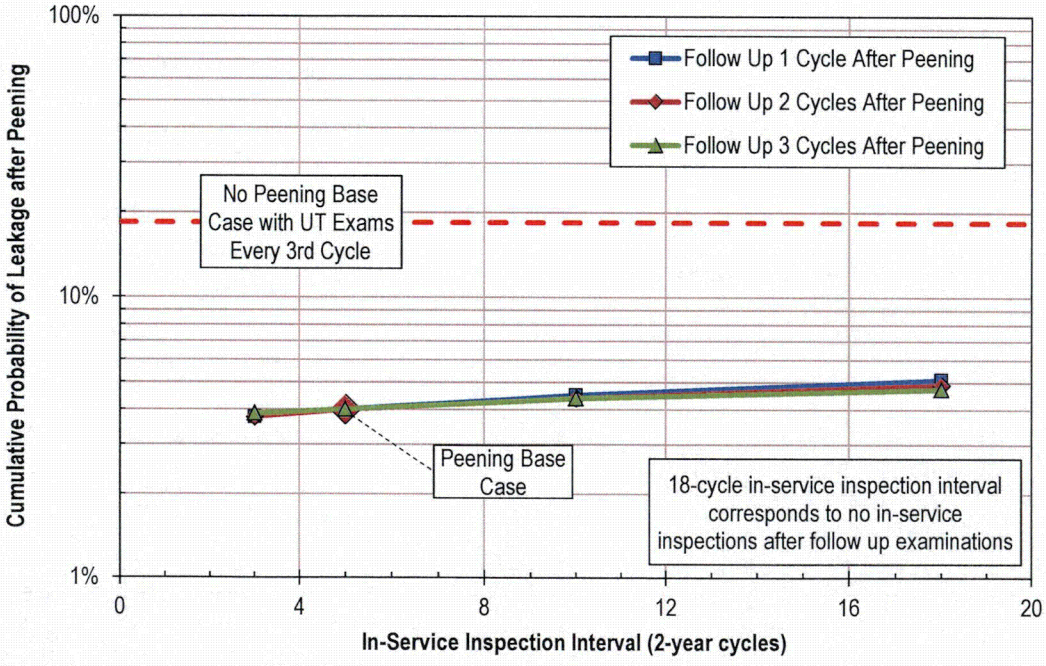

Figure B-33
Cumulative Probability of Leakage from Hypothetical Time of Peening to End of Operational Service Period vs. ISI Frequency for Cold Reactor Vessel Head

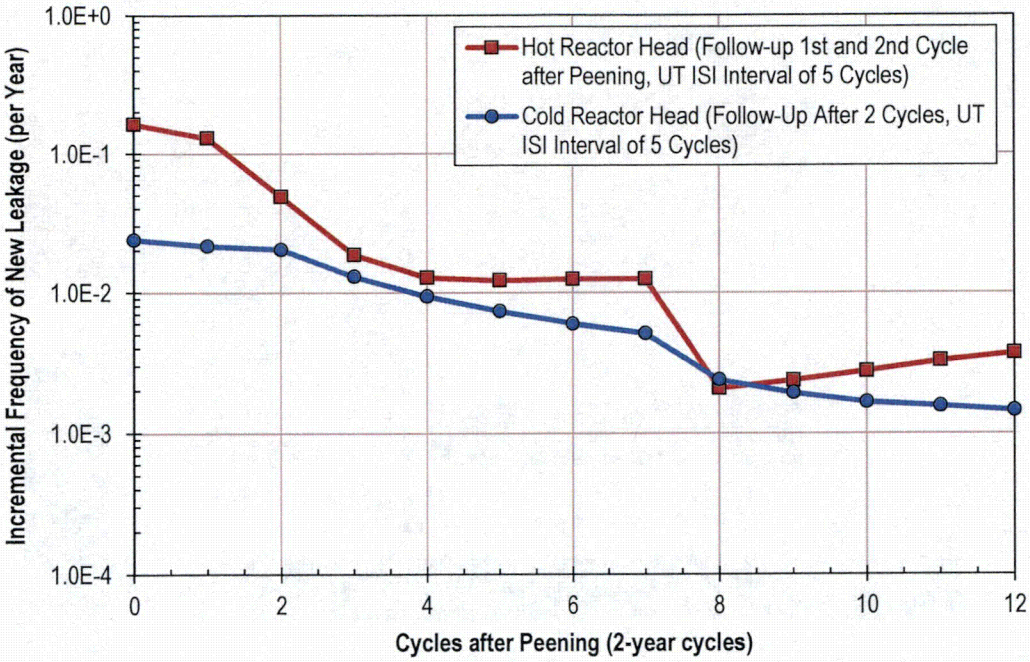

Figure B-34
Incremental Frequency of Leakage after Peening with Relaxed ISI Intervals

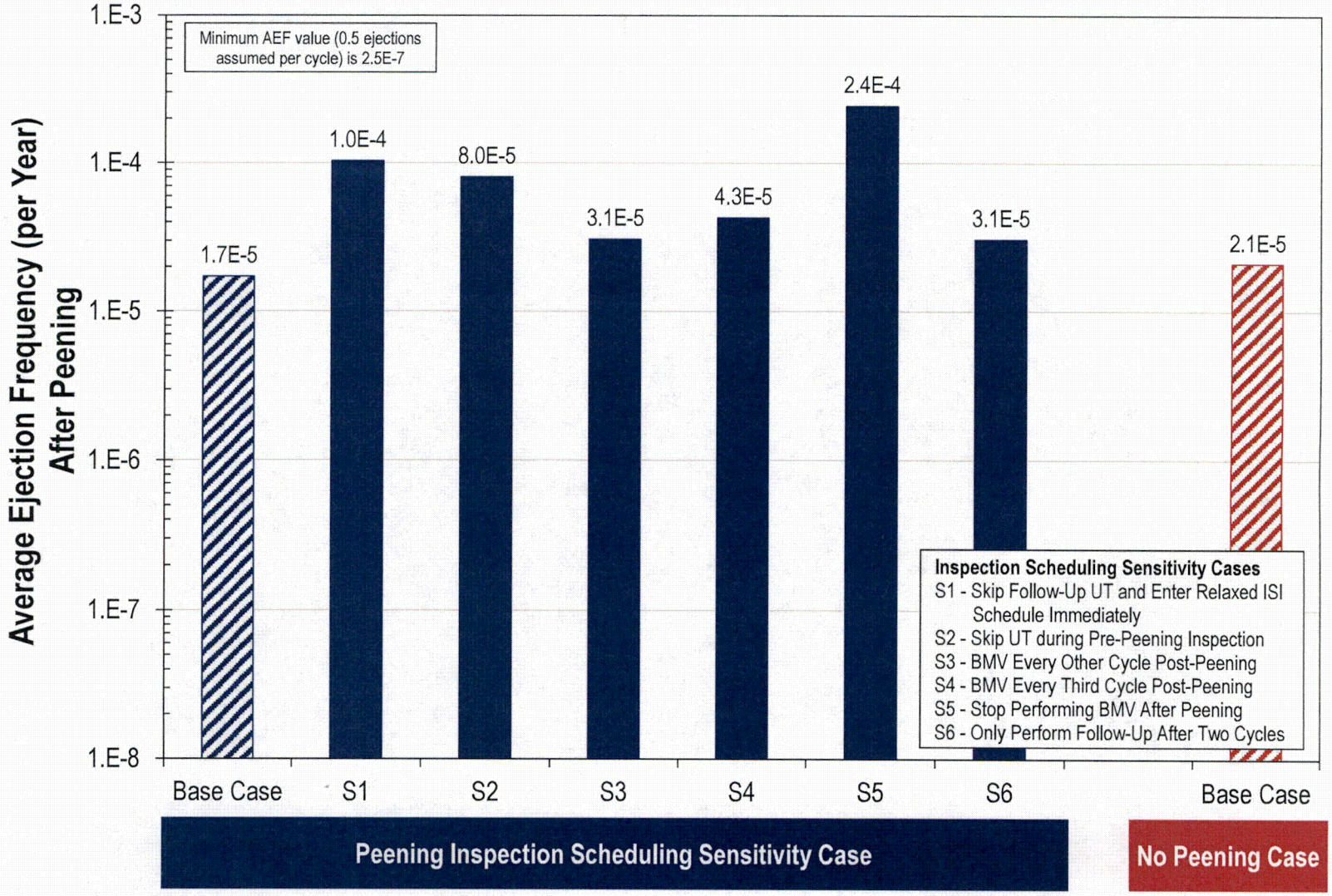

Figure B-35
Summary for Inspection Scheduling Sensitivity Results for Hot RPVHPN Probabilistic Model with Peening

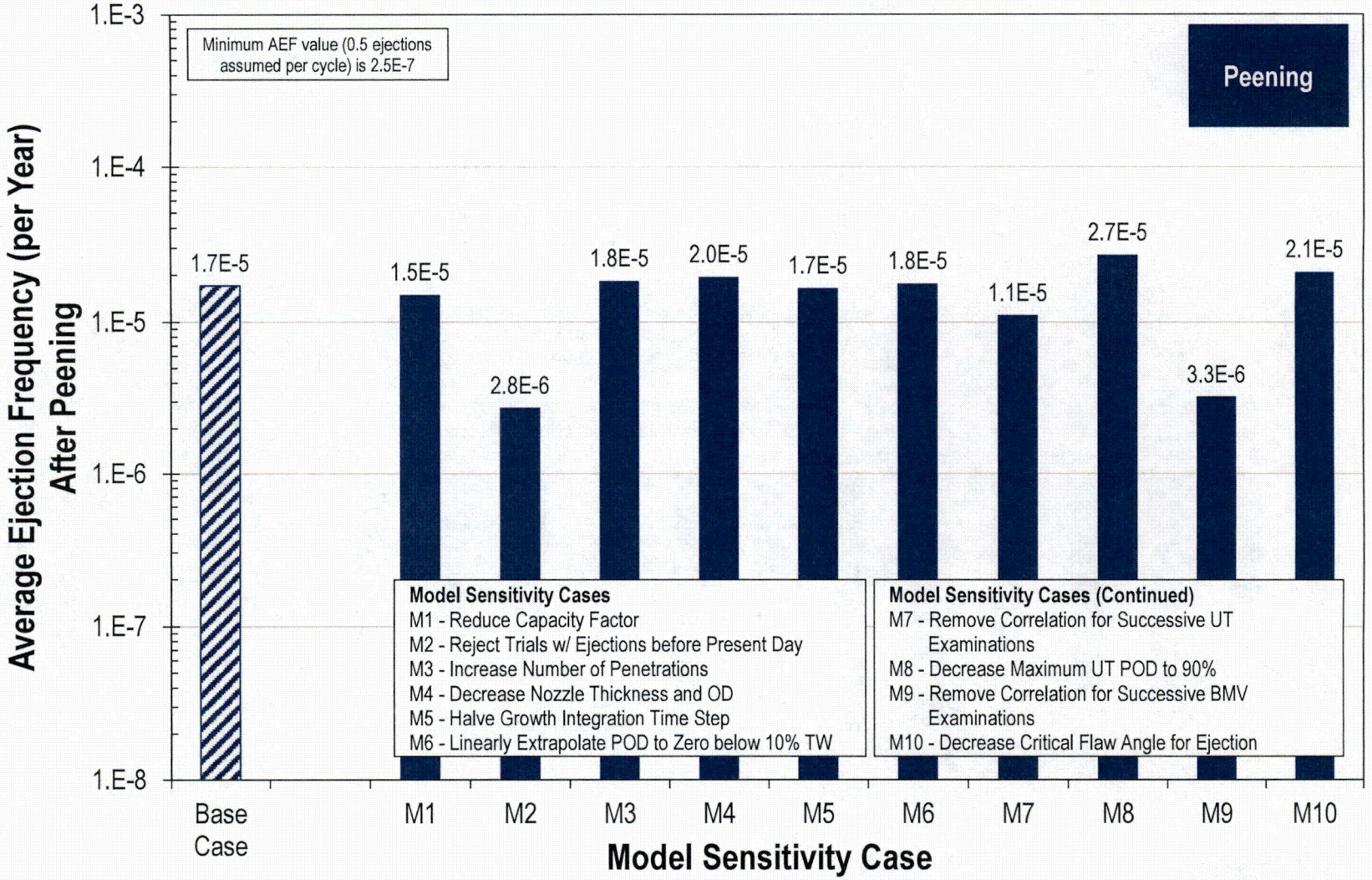

Figure B-36
Summary of Model Sensitivity Results for Hot RPVHPN Probabilistic Model with Peening

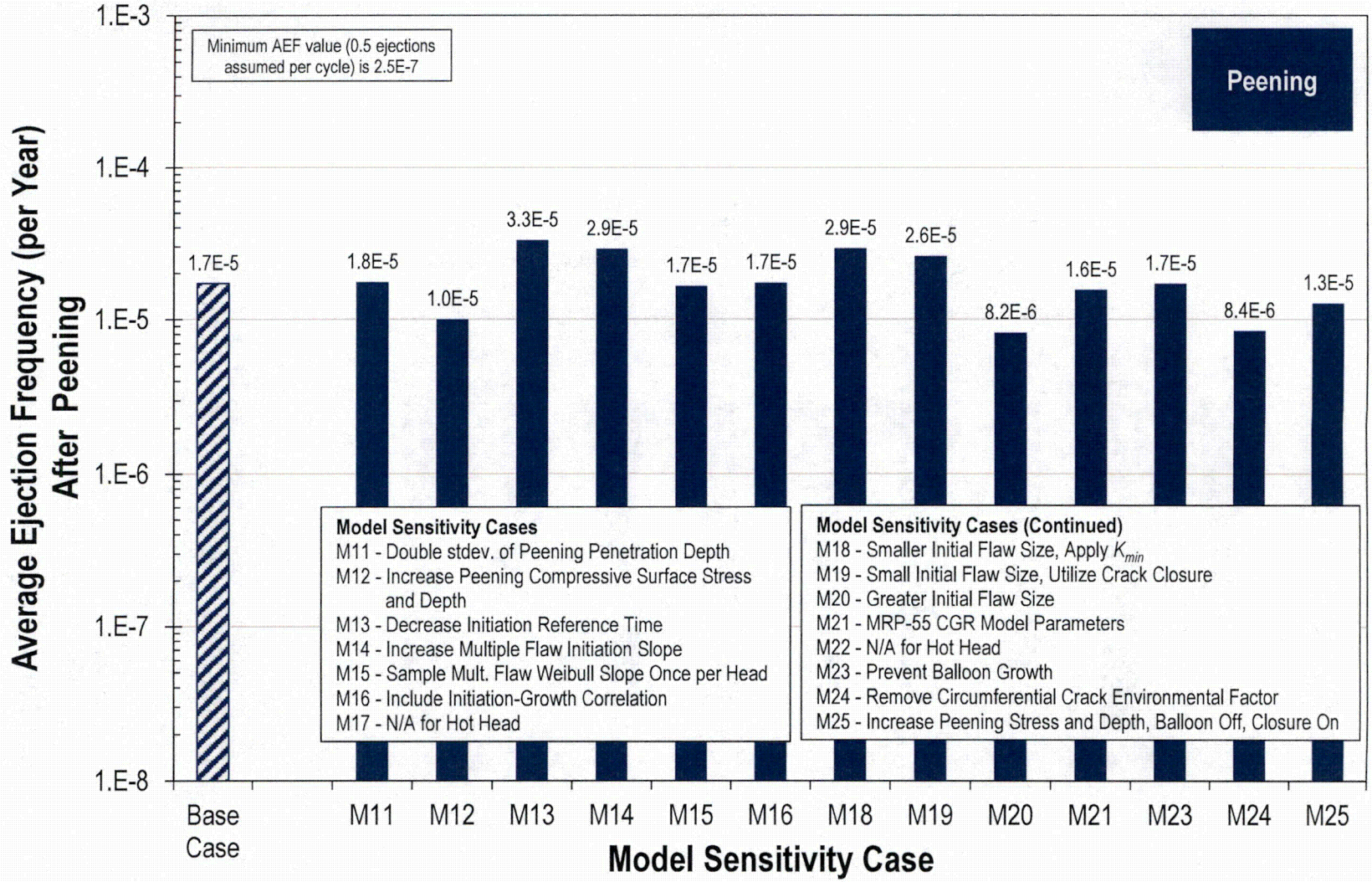

Figure B-37
Summary of Model Sensitivity Results for Hot RPVHPN Probabilistic Model with Peening (continued)

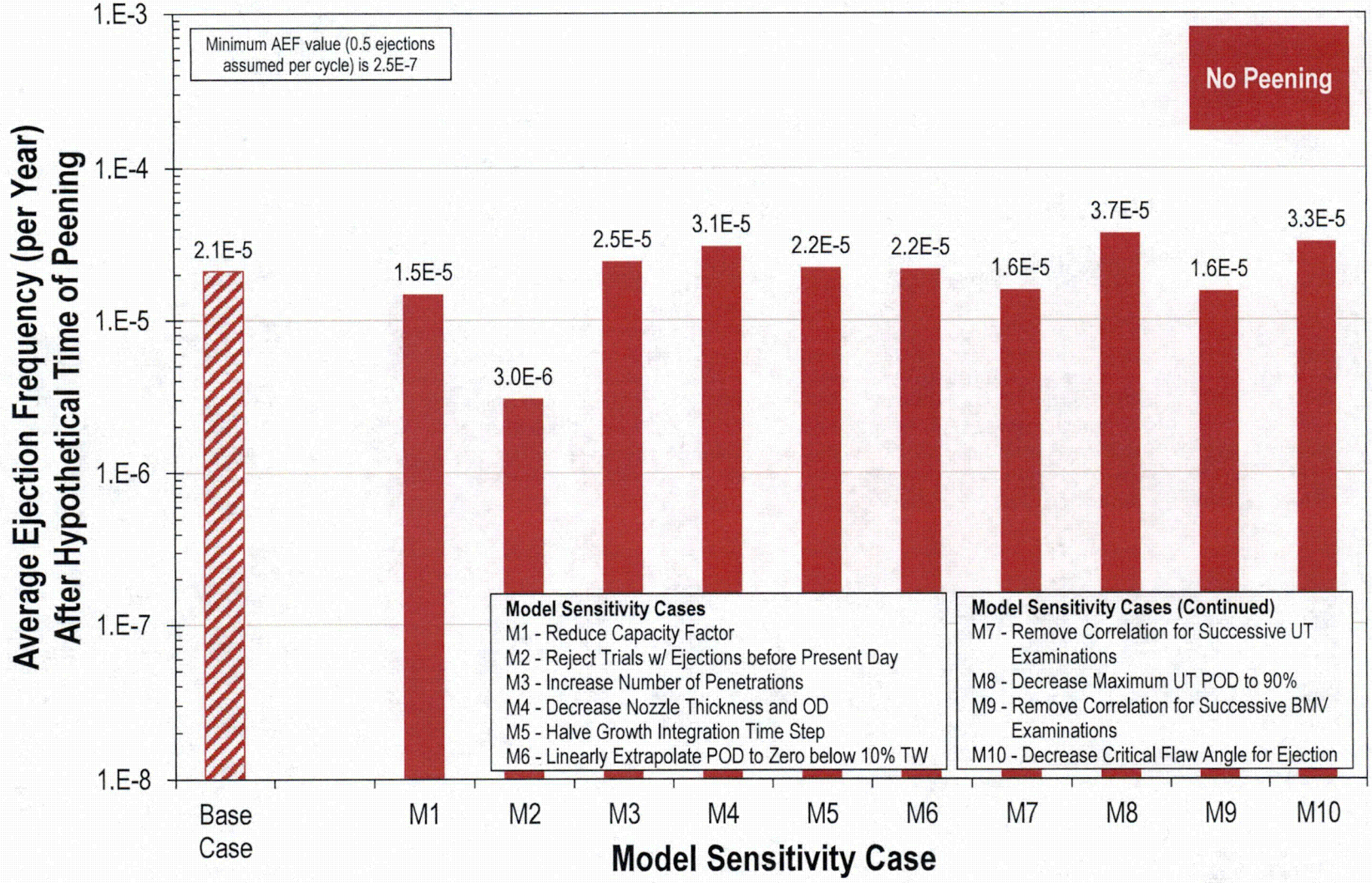

Figure B-38
Summary of Model Sensitivity Results for Hot RPVHPN Probabilistic Model without Peening

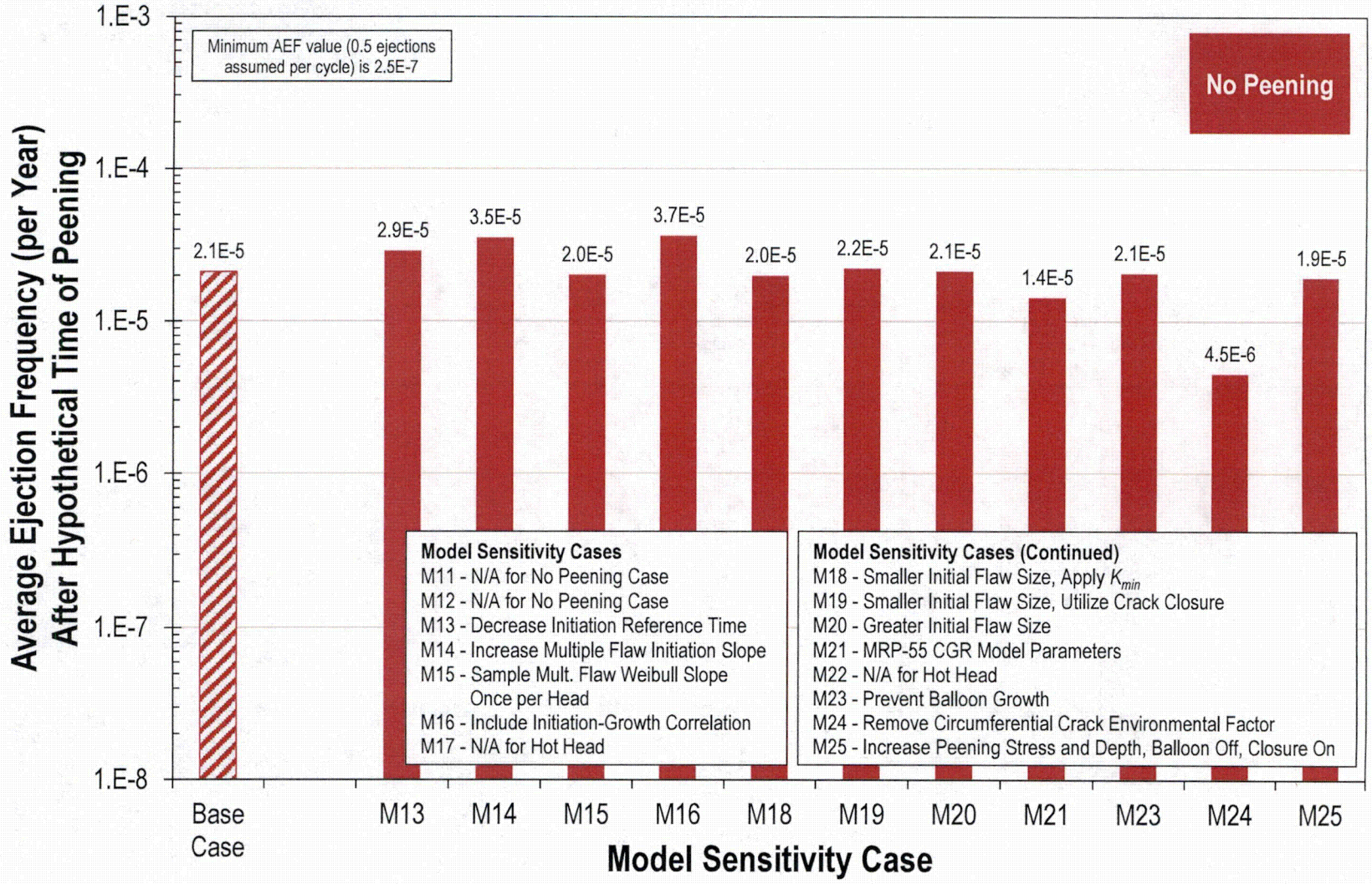

Figure B-39
Summary of Model Sensitivity Results for Hot RPVHPN Probabilistic Model without Peening (continued)

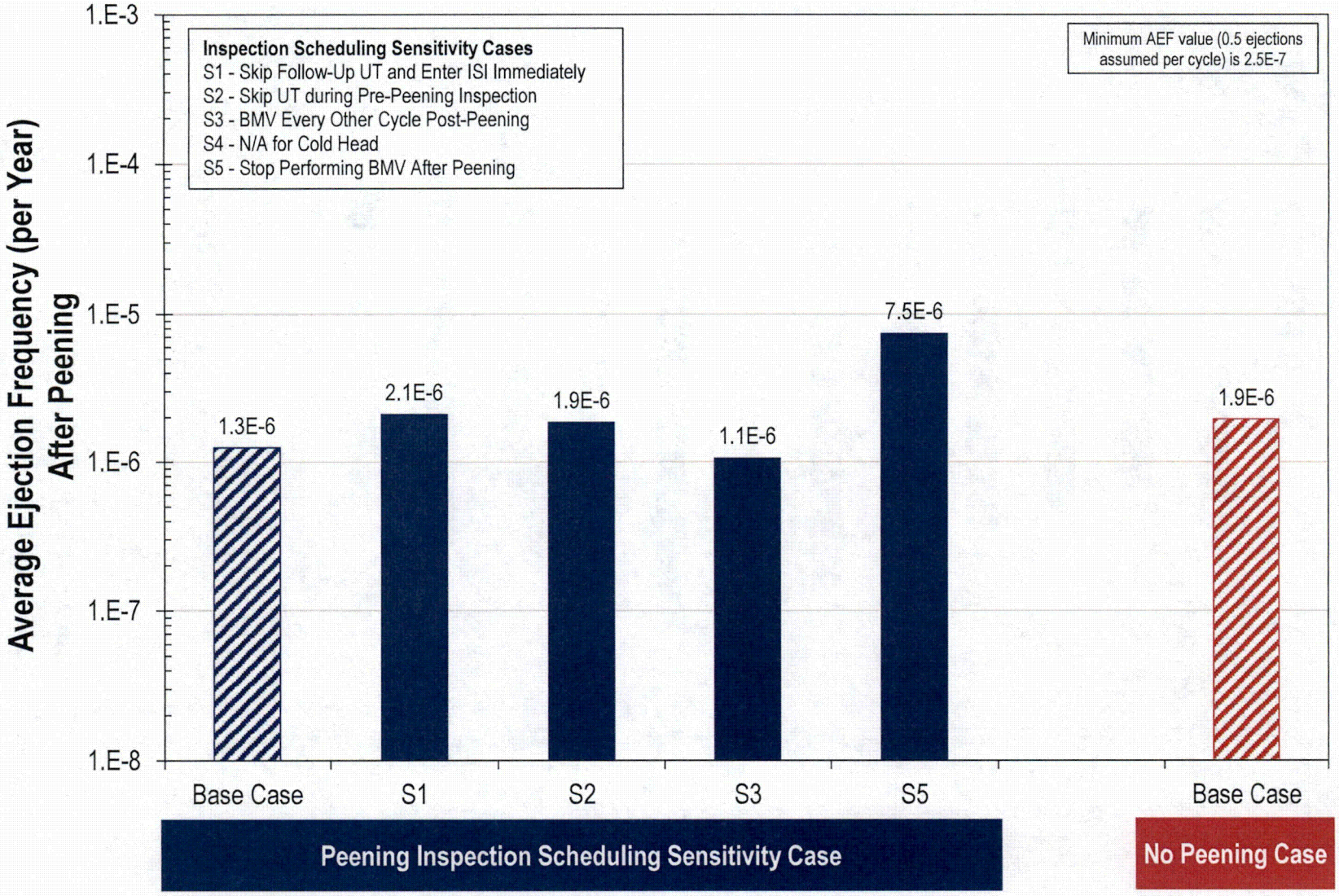

Figure B-40
Summary for Inspection Scheduling Sensitivity Results for Cold RPVHPN Probabilistic Model with Peening

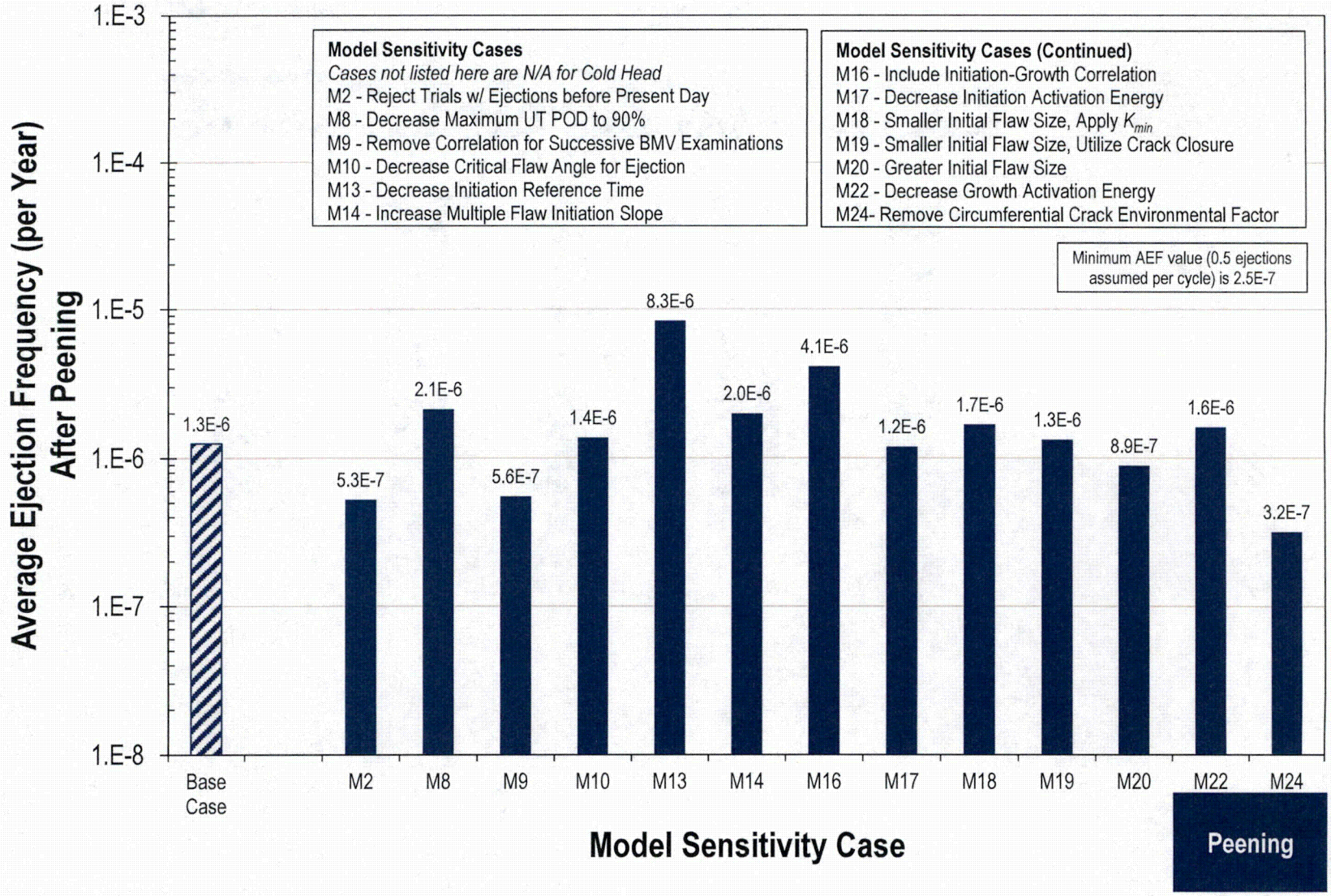

Figure B-41
Summary of Model Sensitivity Results for Cold RPVHPN Probabilistic Model with Peening

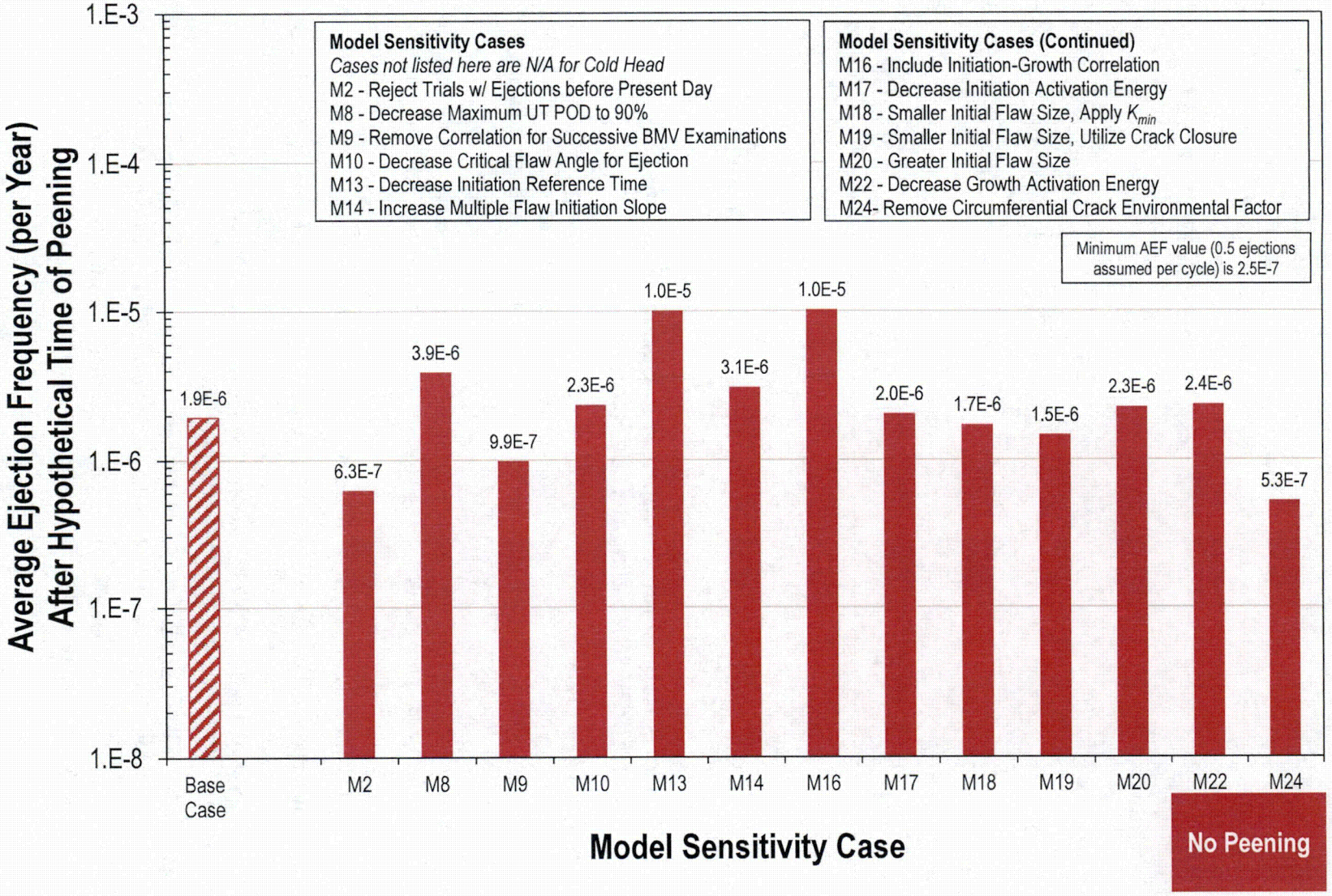

Figure B-42
Summary of Model Sensitivity Results for Cold RPVHPN Probabilistic Model without Peening

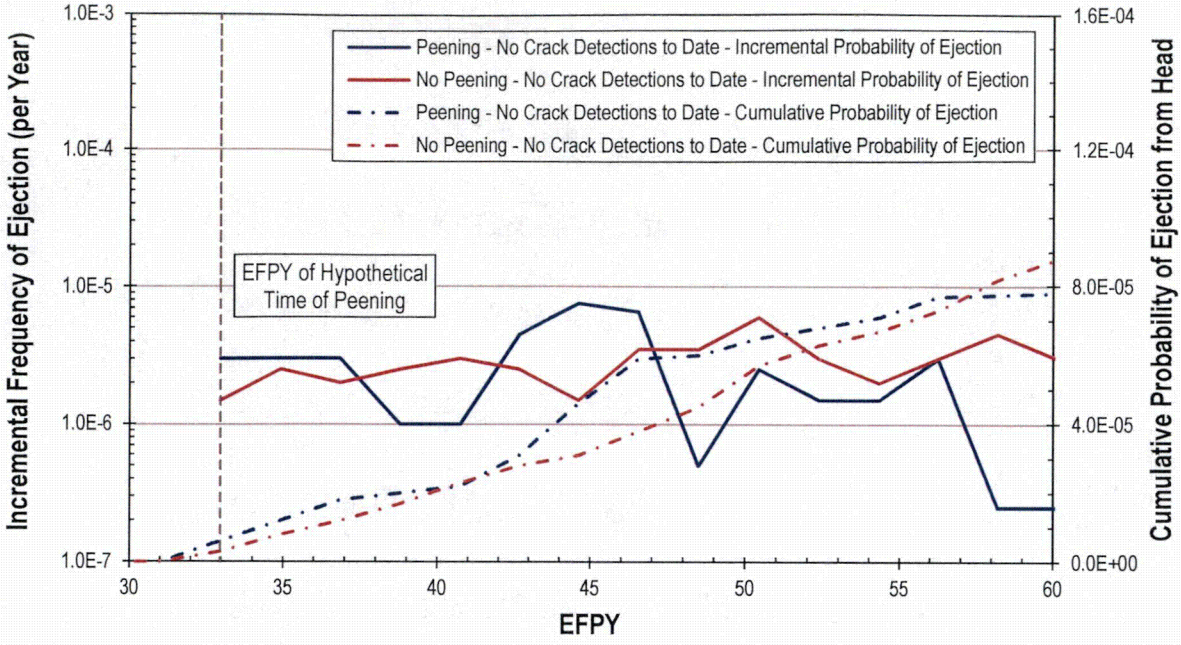

Figure B-43
Prediction of Nozzle Ejection vs. Time for Hot RPVHPNs with No Crack Detections to Date (Model Sensitivity Study 2)

B.10 Conclusions Regarding Appropriate In-Service Examination Requirements for RPVHPNs Mitigated by Peening

The results of the probabilistic analysis of PWSCC on a general hot head support the relaxed UT inspection schedules prescribed in Section 4 of this report. Specifically, cases where the follow-up UT inspection is scheduled for the first and second cycle after peening and subsequent UT inspections are scheduled every 10 years (every interval) result in the following:

- The cumulative leakage probability after the hypothetical time of peening is predicted to be reduced by a factor of approximately 5.5 relative to the unmitigated case per N-729-1.
- The average ejection frequency after the hypothetical time of peening is predicted to be reduced to 81% of the average ejection frequency of the unmitigated case.

The results of the probabilistic analysis of PWSCC on a general cold head support the relaxed UT inspection schedules prescribed in Section 4 of this report. Specifically, cases where the follow-up UT inspection is scheduled two cycles after peening and subsequent UT inspections are scheduled every 10 years (every interval) result in the following:

- The cumulative leakage probability after the hypothetical time of peening is predicted to be reduced by a factor of approximately 4.6 relative to the unmitigated case per N-729-1.
- The average ejection frequency after the hypothetical time of peening is predicted to be reduced to 64% of the average ejection frequency of the unmitigated case.

For both hot and cold leg components, the probabilistic model predicts the rapid decay of incremental leakage probabilities after peening. The calculations also demonstrate the value of visual examinations performed to detect leakage as part of the program of follow-up examinations.

Many key input or modeling assumptions have been varied for Model Sensitivity Cases. The following subset of these cases resulted in an increase in average ejection frequency for the peened component relative to the unmitigated component:

- Hot Model Sensitivity Case 13 – Arbitrarily reducing the initiation reference time by a factor of five results in an AEF of 3.3×10^{-5} for the peened component and an AEF of 2.9×10^{-5} for the unmitigated component. The predicted AEF and ALF for this sensitivity case result in the greatest increase with respect to the base case. However, it is noted that this initiation model results in a prediction of leakage before 20 EFPY in over 95% of hot heads. This is not in line with U.S. PWR operating experience.
- Hot Model Sensitivity Case 18 – Applying a smaller initial flaw size and enforcing a minimum allowable stress intensity factor (regardless of crack size and loading) results in an AEF of 2.9×10^{-5} for the peened component and an AEF of 2.0×10^{-5} for the unmitigated component. The results of this hypothetical case are bounding of the actual stress intensity factors.
- Hot Model Sensitivity Case 19 – Applying a smaller initial flaw size and utilizing crack closure results in an AEF of 2.6×10^{-5} for the peened component and an AEF of 2.2×10^{-5} for the unmitigated component. The reduced initial flaw size provides most of this effect.
- Hot Model Sensitivity Case 21 – Applying the unmodified MRP-55 CGR Model results in an AEF of 1.6×10^{-5} for the peened component and an AEF of 1.4×10^{-5} for the unmitigated component. The predicted AEF for this sensitivity case is less than that of the corresponding base case values.
- Hot Model Sensitivity Case 24 – Removing the circumferential crack environmental factor results in an AEF of 8.4×10^{-6} for the peened component and an AEF of 4.5×10^{-6} for the unmitigated component. The predicted AEF for this sensitivity case is about half of the AEF for the corresponding base case values.
- No Cold Model Sensitivity Cases resulted in a greater AEF for the peened component than for the unmitigated component.
- The average leakage frequencies remain below 0.05 new leaking penetrations per year per head for all peening cases evaluated.

B.11 References

1. *PWR Materials Reliability Program Response to NRC Bulletin 2001-01 (MRP-48)*, EPRI, Palo Alto, CA: 2001. 1006284. [Freely Available at www.epri.com]
2. *PWR Materials Reliability Program, Interim Alloy 600 Safety Assessments for US PWR Plants (MRP-44): Part 2: Reactor Vessel Top Head Penetrations*, EPRI, Palo Alto, CA: 2001. TP-1001491, Part 2.
3. *Materials Reliability Program: Reevaluation of Technical Basis for Inspection of Alloy 600 PWR Reactor Vessel Top Head Nozzles (MRP-395).* EPRI, Palo Alto, CA: 2014. 3002003099. [Freely Available at www.epri.com]
4. ASME Code Case N–729-1, "Alternative Examination Requirements for PWR Reactor Vessel Upper Heads With Nozzles Having Pressure-Retaining Partial-Penetration Welds," Section XI, Division 1, American Society of Mechanical Engineers, New York, Approved March 28, 2006.
5. *Materials Reliability Program: Probabilistic Fracture Mechanics Analysis of PWR Reactor Vessel Top Head Nozzle Cracking (MRP-105NP)*, EPRI, Palo Alto, CA: 2004. 1007834. [NRC ADAMS Accession No.: ML041680489]
6. D. Rudland, J. Broussard, et al., "Comparison of Welding Residual Stress Solutions for Control Rod Drive Mechanism Nozzles," *Proceedings of the ASME 2007 Pressure Vessels & Piping Division Conference: PVP2007*, San Antonio, Texas, July 2007.
7. *Materials Reliability Program Generic Evaluation of Examination Coverage Requirements for Reactor Pressure Vessel Head Penetration Nozzles, Revision 1 (MRP-95R1NP)*, EPRI, Palo Alto, CA: 2004. 1011225. [NRC ADAMS Accession No.: ML043200602]
8. S. Marie, et al., "French RSE-M and RCC-MR code appendices for flaw analysis: Presentation of the fracture parameters calculation – Part III: Cracked Pipes," *International Journal of Pressure Vessels and Piping*, 84, pp. 614-658, 2007.
9. *Technical Basis for RPV Head CRDM Nozzle Inspection Interval H. B. Robinson Steam Electric Plant, Unit No. 2*. Dominion Engineering Inc.: Reston, VA: 2003. R-3515-00-1.
10. *Farley CRDM Through-Wall Circumferential Crack Fracture Mechanics*. Dominion Engineering Inc.: Reston, VA: 2003. C-7781-00-1.
11. *Materials Reliability Program: Crack Growth Rates for Evaluating Primary Water Stress Corrosion Cracking (PWSCC) of Alloy 82, 182, and 132 Welds (MRP-115)*, EPRI, Palo Alto, CA: 2004. 1006696. [Freely Available at www.epri.com]
12. *Materials Reliability Program (MRP) Crack Growth Rates for Evaluating Primary Water Stress Corrosion Cracking (PWSCC) of Thick-Wall Alloy 600 Materials (MRP-55) Revision 1*, EPRI, Palo Alto, CA: 2002. 1006695. [Freely Available at www.epri.com]
13. *Materials Reliability Program: Reactor Vessel Closure Head Penetration Safety Assessment for U.S. PWR Plants (MRP-110NP): Evaluations Supporting the MRP Inspection Plant*, EPRI, Palo Alto, CA: 2004. 1009807. [NRC ADAMS Accession No.: ML041680506]
14. *PWSCC Prediction Guidelines*, EPRI, Palo Alto, CA: 1994. TR-104030.

15. U.S. NRC, Regulatory Guide 1.174, "An Approach for Using Probabilistic Risk Assessment in Risk-Informed Decisions on Plant-Specific Changes to the Licensing Basis," Revision 2, May 2011.

C
TENSILE BALANCING STRESSES IN RESIDUAL STRESS PROFILE IN RESPONSE TO PEENING

C.1 Introduction

C.1.1 Deformation and Tensile Stress Response of Components to Peening

In addition to producing a surface compressive residual stress layer, peening causes deformation of the treated component. Some of the compressive stress at the peened layer is immediately relieved by deformation of the part. As the stiffness of the treated component is assumed to be greater, the resulting deformation decreases, and more of the initial compressive stress at the treated surface is retained.

The retained compressive stress at the peened surface is balanced by residual stresses generated through the component thickness. In order to satisfy static equilibrium, the internal forces and internal bending moments integrated over any cross section through the component must balance to zero or be balanced by a reaction force on the component. If the through-wall stress profile is suitably uniform over a cross section (and the plate length-to-width aspect ratio is suitably large such that beam theory holds), the residual stress profile for an unrestrained flat plate must self-balance by force and through-wall bending moment before and after peening. Thus, the peak balancing tensile stress in the post-peening through-wall profile for an unrestrained flat plate depends on both the force and moment imparted by the surface compressive stress layer.

The balancing stress for peened thick-wall pipes behaves in a similar manner, but the more constrained pipe geometry does not deflect as much as the plate case for equivalent peening compressive stress effect and equivalent wall thickness. As shown in the analyses presented below, the result is that the balancing stress profile for a thick-wall pipe is more nearly uniform than for the case of an unrestrained flat plate of equivalent wall thickness.

C.1.2 Purpose and Approach

The purpose of this appendix is to investigate the magnitude and distribution of tensile stresses developed in response to the peening compressive stresses produced at the treated surface. Any pre-existing flaws located beyond the compressive stress zone would grow during subsequent operation under the influence of these balancing stresses (as well as weld residual stresses and operating stresses).

Specifically, a straightforward linear-elastic finite-element analysis (FEA) approach is taken for flat plate and thick-wall cylinder geometries. Peening is assumed to be applied to a substantial fraction of the plate area or inside diameter surface of a thick-walled cylinder, and the through-wall stress profile developed in the peened region is investigated for different wall thicknesses. The stress source approach ([1], [2], [3]) originally developed to assess the stress effects of shot

peening of a flat plate is applied to calculate the bending stress and axial membrane stress generated in response to peening:

$$\sigma(x) = \sigma_p(x) + \sigma_b(x) + \sigma_a \qquad [C\text{-}1]$$

where:

$\sigma(x)$ = through-wall equilibrium stress profile, as function of through-wall position x

$\sigma_p(x)$ = peening stress source function

$\sigma_b(x)$ = bending stress generated in response to peening (linear function of x)

σ_a = axial membrane stress generated in response to peening

The stress source function, $\sigma_p(x)$, is the stress that would result from peening of an infinitely thick plate. For sufficiently thick plates, the stress source depends only on the peening process applied (i.e., intensity and duration). The form of the stress source function is chosen to fit data for the particular peening process of interest. As described below, published data are used to determine the most appropriate form of the stress source function. Published stress measurements and modeling results also illustrate the expected trends.

The stress source function is imposed in the FEA model as an initial condition for the stress state in the region of the "peened" surface, and the FEA solver is used to calculate the equilibrium stress response. The two-dimensional FEA model for the unrestrained flat plate case is used to demonstrate how more of the compressive stress near the surface is retained as the wall thickness is increased for a constant peening intensity (i.e., stress source function). Additional cases for the flat plate geometry show how the equilibrium stress profile, including the peak tensile stress, varies with wall thickness while holding constant the amount of compressive stress retained at the "peened" surface (surface magnitude and compressive depth) by varying the stress source function. These results are then extended to the thick-wall cylinder geometry.

The form of the stress source function is validated based on a published set of experimental stress measurements performed on a peened flat plate. The FEA approach is further validated through application of a simple bilinear stress profile that is analytically constrained to satisfy through-wall force and moment balances.

The FEA model is described in Section C.2, the simulated cases are listed in Section C.3, the results are presented in Section C.4, and the model validation is presented in Section C.5. Conclusions are made in Section C.6.

C.1.3 Relevant Literature

Researchers have studied tensile balancing effects in post-peening residual stress profiles in a range of geometries for shot peening, laser peening, and water-jet peening. The following findings are relevant to the tensile balancing stress in the post-peening residual stress profile:

- Buchannan and John [4] show that for a constant residual surface stress, the peak tensile stress decreases as component thickness increases. With increased component thickness, the

balancing force is spread over a greater distance and the difference in balancing tensile stress required to develop a balancing through-wall moment is decreased.

- Hill, et al. [5] show that the peak tensile stress indirectly induced by a peening process decreases as the compressive residual stress at the surface decreases. As the peening intensity is increased and a larger compressive surface stress is produced, the peak tensile stress beyond the compressive layer tends to increase.
- Menig, et al. [6] investigated the nature of the tensile stress field beyond the peening compressive layer. The results presented in this paper indicate that the compressive residual stresses generated by peening are balanced by rather low tensile residual stresses extending over the whole cross-section of the component.
- DeWald and Hill [7] measured stresses and performed strain and stress modeling for four different specimen geometries treated by laser peening, including thick-wall cylinders peened on the outer diameter. The through-wall residual stress measurements were made using the contour method. The stress profile measured for the thick-wall cylinder case is comparable to that observed in other studies for peening of flat plates, although the profile near the inside surface (not peened) showed greater curvature than for flat plate cases. This case is not directly applicable to peening of reactor vessel primary nozzles because the peening was performed on the OD and because of the especially small inner-radius-to-thickness ratio, R_i / t = 15 mm / 15 mm = 1.0.

C.2 ANSYS Model Description

A two-dimensional linear-elastic ANSYS [8] FEA model is used to simulate the balancing stress effects of either:

(1) a cross section of a flat plate peened on one side, or

(2) a thick-wall pipe that is subjected to axisymmetric peening on the pipe inside surface.

The peening process itself is not simulated. Instead the balancing stress profile generated in response to the peening compressive stress layer at the treated surface is calculated considering the effect of the component geometry and stiffness. The standard peening stress source approach, also known as the "eigenstress" approach, is taken in which the initial stress profile due to peening (prior to deformation of the component and development of the balancing stress) is directly input to the model as an initial condition. This initial stress source function is independent of the component geometry given a sufficiently large wall thickness. The final stress state at equilibrium, which reflects both the reduction in peening compressive stress due to component deformation as well as generation of the balancing residual stress, is calculated using the ANSYS FEA solver. Although the peening process itself results in substantial local yielding and plastic strains, the redistribution of stress beyond the surface compressive residual stress zone in response to peening is an elastic unloading problem [1], and thus amenable to the linear-elastic stress source approach.

The material properties, geometry, boundary conditions, and loading are described in the following subsections.

C.2.1 Material Properties

The ANSYS model is a linear-elastic model. Thus the needed properties are limited to Young's Modulus and Poisson's Ratio. As shown in Table C-1, room-temperature values were input using the physical properties tabulated in Section II Part D of the ASME Boiler and Pressure Vessel Code [9] for Alloy 600 and another nickel-based alloy, Alloy 22. The material properties for Alloy 22 were applied in the case used to validate the chosen form of the stress source function.

Table C-1
Material Properties [9]

Material	Parameter	Units	Value
Alloy 600	Young's Modulus	Pa	2.13E+11
	Poisson's Ratio	-	0.31
Alloy 22	Young's Modulus	Pa	2.06E+11
	Poisson's Ratio	-	0.31

C.2.2 Geometry

The same two-dimensional mesh is used to model a flat plate or an axisymmetric pipe. The ANSYS PLANE183 element type is applied under the generalized plane strain assumption for the flat plate geometry and in axisymmetric mode for the pipe geometry.

It was shown that the choice of either generalized plane strain or plane stress for the plate geometry does not significantly affect the in-plane stress results presented in this appendix. The reason is that the calculated profile for the in-plane (Y-direction) stress must satisfy the same force and moment balances regardless of whether the plane strain or plane stress assumption is made for two-dimensional treatment of Hooke's Law.

The geometry of the plate and pipe models is defined by the example mesh shown in Figure C-1. When modeling a plate, the model can be considered to be infinitely wide in the out-of-plane direction. When modeling a pipe, the out-of-plane direction is the azimuthal dimension and the axis of rotation is to the left of the mesh of Figure C-1. The pipe geometry boundary conditions make the pipe behave as though it is infinite in length. As shown in red in this figure, the model includes a distinct area on the left (inner diameter) surface where the stress source function is applied to simulate the effects of peening. This area is assigned an initial stress profile, as described by Section C.2.4, to model the effects of peening while the initial stress state in the remainder of the mesh is zero.

The mesh spacing is controlled in the model to ensure the results are accurate in the areas of interest. The mesh is refined in the region where the stress source function is applied because this is the area with the largest stress gradient. The effect of overall mesh refinement was checked to confirm model convergence. The length of the peened area is chosen to result in a region of reasonably uniform stresses that are reasonably fully developed without edge effects, and the solution is confirmed to be converged with respect to the modeled length of the mesh. The modeled geometry satisfied a study of the spatial uniformity of the peak stress and of the compressive stress layer depth.

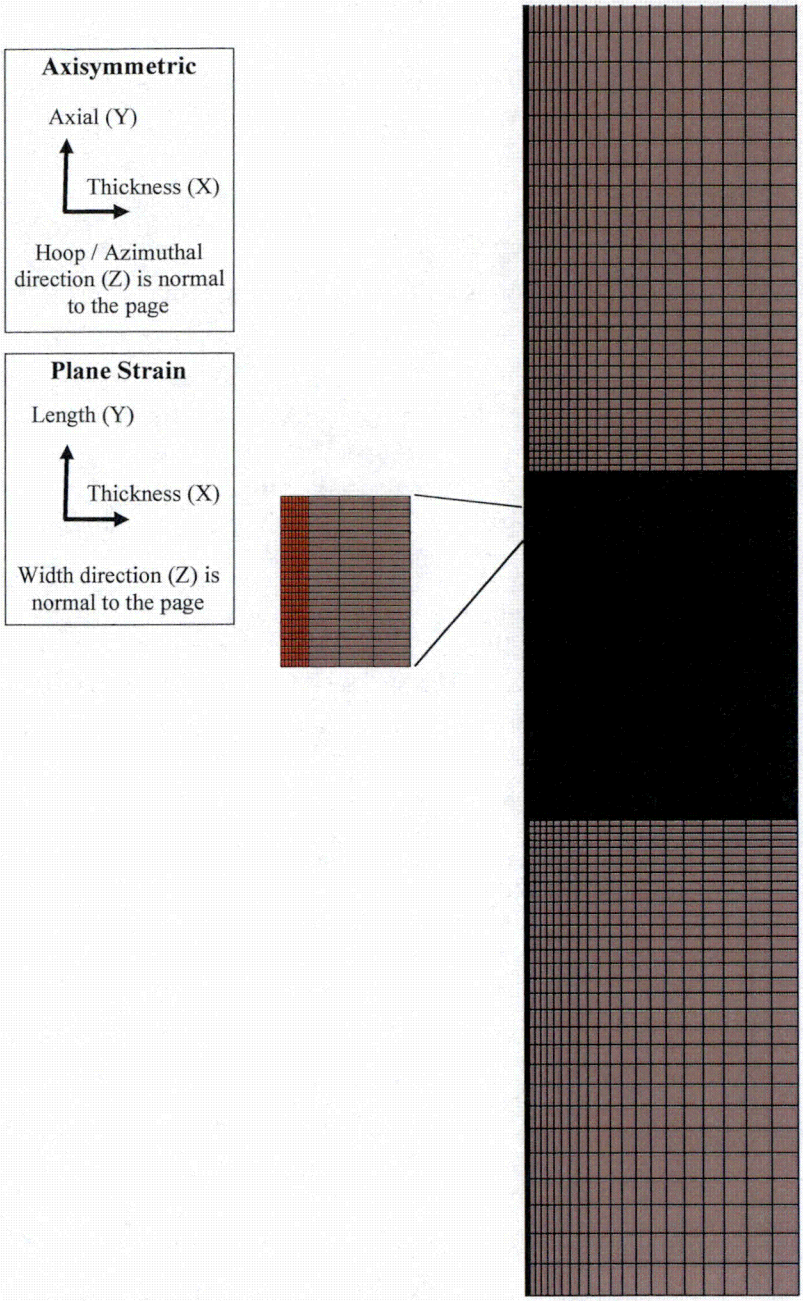

Figure C-1
Example Mesh with Region of Application of Stress Source Function in Red (wall thickness = 63.5 mm)

C.2.3 Boundary Conditions

To prevent rigid-body motion of the model, the following boundary conditions are applied:

Flat Plate Geometry

- Midpoint of Left Side of Cross Section: Zero displacement in the X- and Y-directions
- Midpoint of Right Side of Cross Section: Zero displacement in the Y-direction

Thick-Wall Pipe Geometry

- Bottom Row of Nodes: Zero displacement in Y-direction
- Top Row of Nodes: Displacement in Y-direction is uniformly the same (coupled)

C.2.4 Loading

The only load source in the model is the biaxial initial stress state specified in the region where the stress source function is applied. The initial stress state is specified using the ANSYS INISTATE command and applied to the nodes of the elements in the stress source region according to the nodal position. The profile is applied to both the SY and SZ stress components. No initial stress is input for the through-thickness component (SX).

Per the validation exercise described below in Section C.4.1, the stress source function is assumed to have an exponential form. An improved fit to the validation data resulted from a small refinement to a pure exponential decay function. The stress source function is based on an exponential function scaled to reach zero at a depth of δ_p:

$$\sigma_p(x) = \sigma_{p,0}\left[\frac{e^{-x/\tau} - R}{1-R}\right] \quad \text{for } x < \delta_p \qquad \text{[C-2]}$$

$$\tau = -\frac{\delta_p}{\ln(R)}$$

where:

δ_p = depth of region subjected to initial stress source function

x = through-wall depth from "peened" surface

$\sigma_p(x)$ = peening stress source function

$\sigma_{p,0}$ = initial peening compressive stress at peened surface prior to deformation

R = fraction of exponential remaining at $x = \delta_p$, taken to be 0.04 based on the comparison in Section C.4.1

Examples of a stress source function having the form of Equation [C-2] and the final equilibrium stress state in the component are shown in Figure C-2 and Figure C-3.

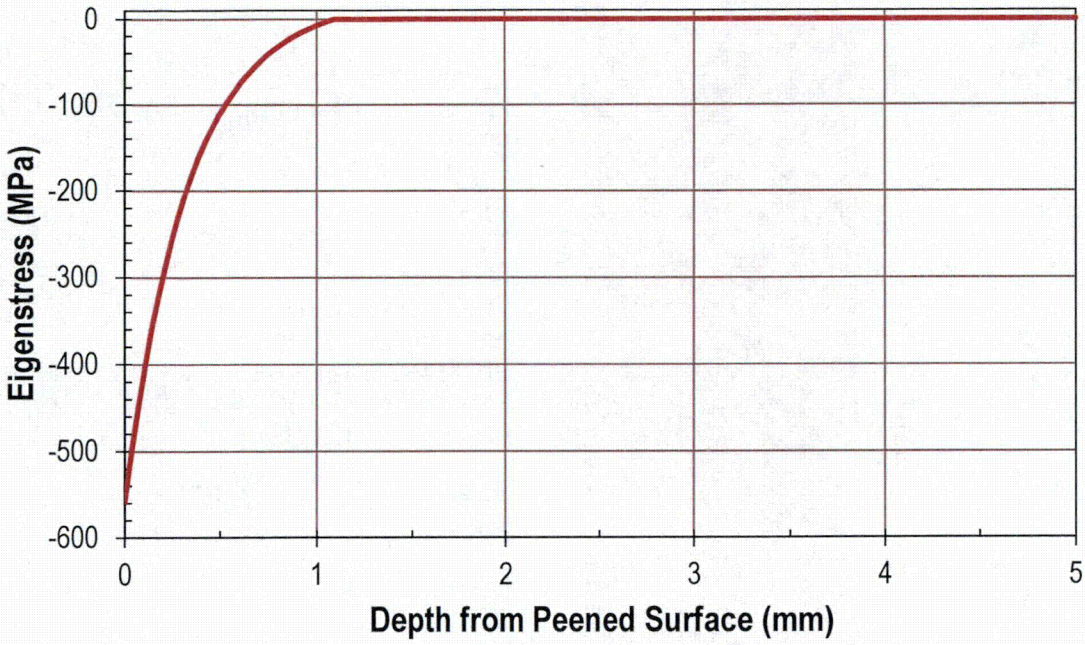

Figure C-2
Example Stress Source Function for $\sigma_{p,0}$ = -558 MPa (-80.9 ksi) and δ_p = 1.09 mm (0.043 in.)

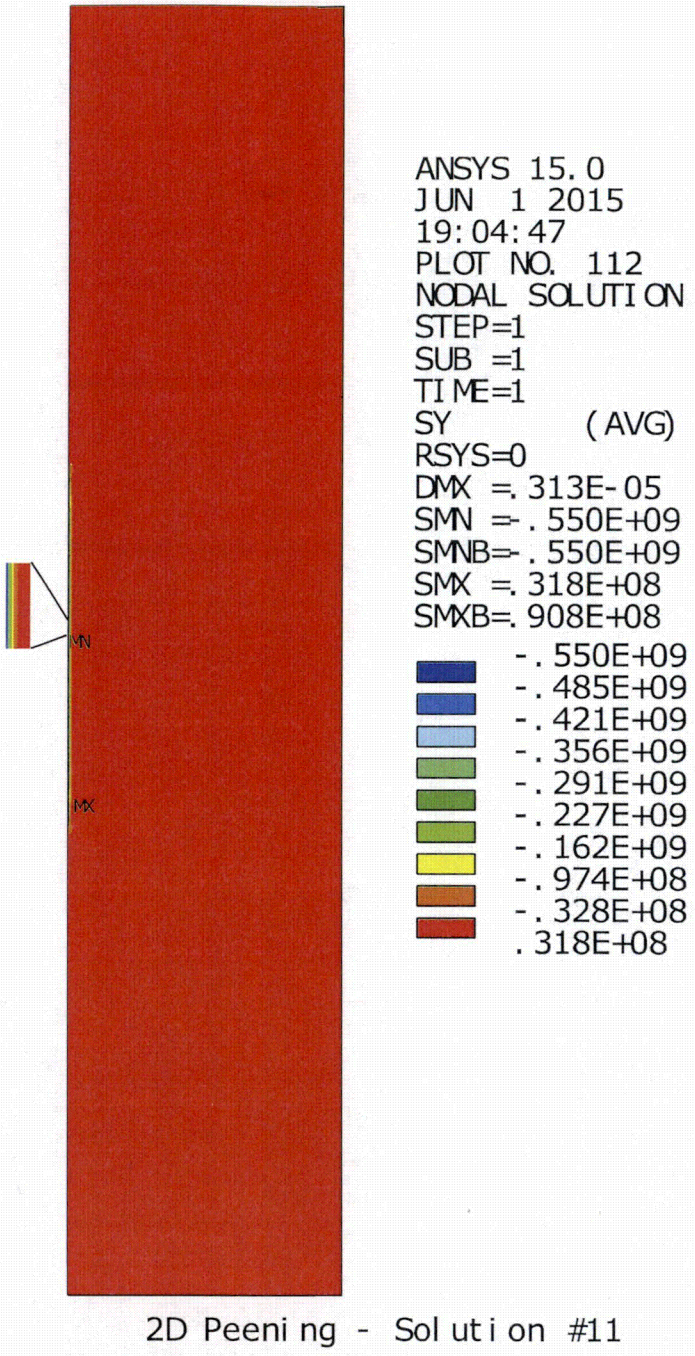

Figure C-3
Example Equilibrium Stress Solution Contour Plot for the Length (Y) Direction Stress (SY) for Flat Plate Model (wall thickness = 63.5 mm)

C.3 ANSYS Model Cases

The FEA model was used to investigate the following cases:

- **Validation of Exponential Form of Stress Source Function**
  - Simulates the stress profile for a flat plate treated by laser peening (measured by Hill et al. [5]) (Figure C-4)
  - Material: Alloy 22
  - Plate with thickness of 20 mm and length of 38 mm
  - Peened area length of 30 mm
  - Modeled using an equilibrium surface compressive stress of ~470 MPa (68.2 ksi) and depth of 2.74 mm
- **Plate with Thickness of Reactor Vessel Outlet Nozzle (Two-Dimensional)**
  - Simulates an unrestrained flat plate with thickness comparable to the reactor vessel outlet nozzle pipe case to show the effect of modeling a plate vs. a pipe. The simpler plate geometry is a common geometry for published testing and modeling efforts.
  - Material: Alloy 600
  - Plate length of 300 mm and peened area length of 80 mm
  - Plate wall thickness:
    - Base case thickness of 2.5 inches (63.5 mm), which is close to the lower bound thickness of 2.4 inches (61 mm) cited in MRP-109 [10]
    - Sensitivity cases illustrating effect of wall thickness ranging from a factor of 8 thinner to a factor of 6 thicker
  - Peening stress source function assumptions:
    - Constant stress source function ($\sigma_{p,0}$ = -558 MPa (-80.9 ksi) and δ_p = 1.09 mm) to illustrate greater retention of initial compressive stress as thickness is increased
    - Vary stress source function to obtain equilibrium surface compressive stress of ~550 MPa (80 ksi) and compressive stress depth of 1.0 mm
- **Reactor Vessel Outlet Nozzle (Axisymmetric)**
  - Simulates effects of peening on the ID of a thick-wall pipe with the dimensions of a typical reactor vessel outlet nozzle (RVON) dissimilar metal weld.
  - Material: Alloy 600
  - Pipe length of 300 mm, peened area length of 80 mm, and ratio of inner radius to thickness of 5.8 (yields an outer diameter of 34 inches (864 mm) for a thickness of 2.5 inches (63.5 mm))
  - Pipe wall thickness:
    - Base case thickness of 2.5 inches (63.5 mm), which is close to the lower bound thickness of 2.4 inches (61 mm) cited in MRP-109 [10]
    - Sensitivity cases illustrating effect of wall thickness ranging from a factor of 8 thinner to a factor of 6 thicker (evaluated both for a constant outer diameter of 34 inches and for a constant ratio of inner radius to wall thickness of 5.8)

- Peening stress source function assumptions:
  - Vary stress source function to obtain equilibrium surface compressive stress of ~550 MPa (80 ksi) and compressive stress depth of 1.0 mm
  - Sensitivity cases illustrating effect of compressive stress depth using 0.5 mm and 1.5 mm equilibrium surface compressive stress depths for RVON base case dimensions

C.4 ANSYS Model Results

C.4.1 Validation of Exponential Form of Stress Source Function

The parameters for the exponential stress source function ($\sigma_{p,0}$ and δ_p in Equation [C-2]) were varied until the match between the measured stress profile and the calculated equilibrium profile in Figure C-4 was obtained. The magnitude of the peak stress obtained in this case reflects the magnitude of the compressive stress depth (2.7 mm) in comparison to the wall thickness (20 mm).

The very good agreement between the measured and predicted stress profiles shows that the exponential form of Equation [C-2] is a good choice to model the peening effect for the type of laser peening performed by Hill et al. [5]. Furthermore, the measured peening compressive stress profiles presented in MRP-267 Rev. 1 [11] for a variety of laser peening and water jet peening processes have shapes that are generally reasonably approximated by the shape of the peening compressive stress profile measured by Hill et al. [5] and shown in Figure C-4. Hence, the stress source functional form defined in Equation [C-2] is applied in all the FEA cases.

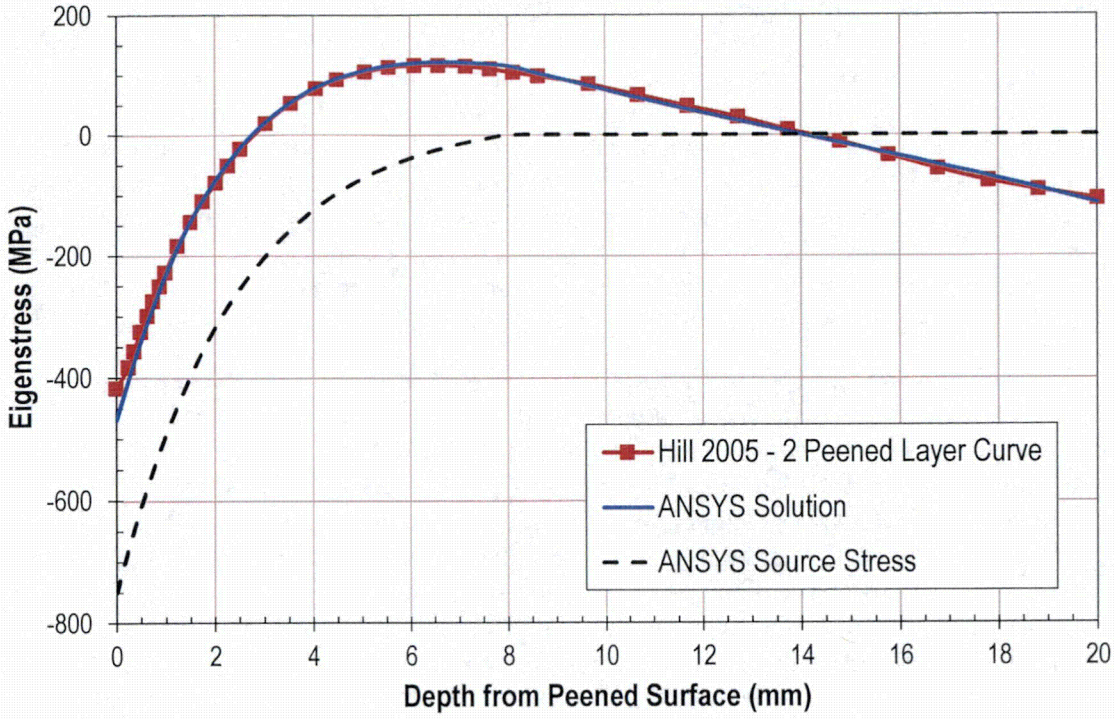

Figure C-4
Validation of Exponential Form of Stress Source Function Using Through-Wall Stress Profile Measured by Hill et al. [5]

C.4.2 Calculated Stress Profiles for Flat Plate and Thick-Wall Pipe Geometries

The FEA analyses results are shown in Figure C-5 through Figure C-13, where in each figure the stress profile is taken at the midpoint of the peened region (i.e., the symmetry plane of the model):

Effect of Wall Thickness on Retained Peening Compressive Stress (Flat Plate)

- Figure C-5 illustrates how the compressive stress effect developed by peening increases (in terms of surface compressive stress magnitude and compressive stress depth) for the same peening intensity as the wall thickness is increased. More of the initial peening compressive stress would be retained for the thick-wall pipe geometry for equivalent wall thickness because of its greater level of constraint. Because the peening performance criteria are based on the stress profile achieved following peening (including the relaxation in compressive stress at the surface due to elastic deformation of the component upon peening), the results presented below for a consistent equilibrium compressive stress effect are more important to the conclusions of this investigation.

Effect of Wall Thickness on Balancing Stress Profile (Flat Plate and Thick-Wall Pipe)

- Figure C-6 clearly illustrates how the peak tensile stress is reduced as the wall thickness is increased for the flat plate geometry with the stress source function parameters varied to obtain constant equilibrium values of the surface compressive stress magnitude and compressive depth. The profiles show how a linear stress profile (through-wall bending) and an axial membrane stress component are produced in response to the peening effect. As discussed by Bernasconi and Roth [1], this is the expected behavior of a peened plate and reflects simple beam behavior. Note that it was numerically confirmed that these calculated stress profiles satisfy both force and moment balance. This is a requirement of the model since the through-thickness profile for stress in the Y-direction is necessarily uniform in the Z-direction (into the page) given the two-dimensional assumption.
- Figure C-7 shows similar behavior for the axial stress profile for the thick-wall pipe geometry. For equivalent wall thickness, the peak tensile stress is smaller for the pipe axial stress case. The pipe geometry is more constrained than a flat plate and does not deflect as much as the plate case for equivalent peening compressive stress effect and equivalent wall thickness. The reduced curvature for the pipe case means that a smaller through-wall bending stress component is produced in the axial direction than would be the case for the corresponding flat plate. In addition, the gradient in cross sectional area between the inner and outer portions of the pipe cross section tends to increase the contribution of a given through-wall stress gradient to the through-wall force and bending moment in comparison to the situation for a flat plate. Note that it was numerically confirmed that these calculated stress profiles satisfy force balances. Force balance over a given through-wall profile is a requirement of the model since the axial stress profile is necessarily uniform in the azimuthal direction given the axisymmetric assumption. The pipe geometry does not satisfy the moment balance in the same manner as for the unrestrained flat plate as shear stresses contribute to the balance for the pipe.
- While the results in Figure C-7 represent a constant outer diameter while the thickness is varied, Figure C-8 plots the equivalent axial stress results for a constant inner-radius-to-thickness ratio. The peak tensile stress for the pipe geometry cases remains smaller than the peak tensile stress in the plate geometry case for equivalent wall thickness. Note that the curves with a positive slope in Figure C-8 have a lower peak tensile stress than the equivalent constant outer diameter curves (having a negative slope). These cases with positive slope correspond to relatively small wall thicknesses and are the result of a more complex deformed shape of the pipe compared to cases with greater wall thickness or greater diameter. It was numerically confirmed that these calculated stress profiles also satisfy force balance.
- Figure C-9 and Figure C-10 show the calculated profiles for the case of the hoop stress for the thick-wall pipe geometry. Note that the compressive stress depth at equilibrium for the hoop stress profile varies slightly for the different thickness cases because the stress source function was varied to maintain the compressive stress depth for the axial stress profile. Regardless of this point, the magnitude of the tensile stress response is substantially smaller for the hoop stress profile in comparison to that for the axial stress for equivalent wall thickness. This lower peak magnitude occurs because the force balance in the hoop direction is enforced over the entire modeled area, permitting a

distribution of the tensile balancing stress over a greater area. The hoop profiles have smaller slopes than the axial profiles because the axial change in curvature upon peening is greater than the change in curvature of the pipe in the circumferential direction. The pipe geometry is most constrained in the circumferential direction.

Effect of Wall Thickness on Peak Balancing Tensile Stress (Flat Plate and Thick-Wall Pipe)

- Figure C-11 and Figure C-12 plot the peak tensile stress of the profiles in Figure C-6 through Figure C-10 directly as a function of wall thickness. The peak tensile stress is plotted as a percentage of the surface compressive stress value as the shape of the stress profile does not depend on the magnitude of the surface compressive stress.

Effect of Peening Compressive Stress Depth on Balancing Stress Profile (RVON Pipe Geometry)

- The results in Figure C-6 through Figure C-12 assumed a post-peening compressive stress depth of 1 millimeter. Figure C-13 illustrates how the axial stress profile for the RVON geometry is affected by this assumption. Profiles are shown for compressive depths of 0.5 mm and 1.5 mm in addition to 1.0 mm. The magnitude of the peak tensile stress has an approximate linear dependence on the compressive stress depth. This is expected given that the force and moment created by the compressive profile close to the peened surface are each approximately proportional to the compressive depth.

As shown in the figures, the calculated maximum tensile stress for a given peening compressive stress effect (surface magnitude and compressive depth) decreases with increasing wall thickness. This applies in both the axial and hoop directions for the pipe.

For the reactor vessel outlet nozzle (RVON) thick-wall pipe geometry, the peak tensile balancing stresses are less than about 2% of the magnitude of the compressive surface stress for the case of a compressive stress layer at the pipe ID that is 1 millimeter deep. This relatively small magnitude for the peak tensile balancing stress is the result of the balancing force and moment being spread over the large wall thickness of this component, plus the fact that the pipe geometry is more constrained than a flat plate and does not deflect as much as the plate case for equivalent peening compressive stress effect and equivalent wall thickness.

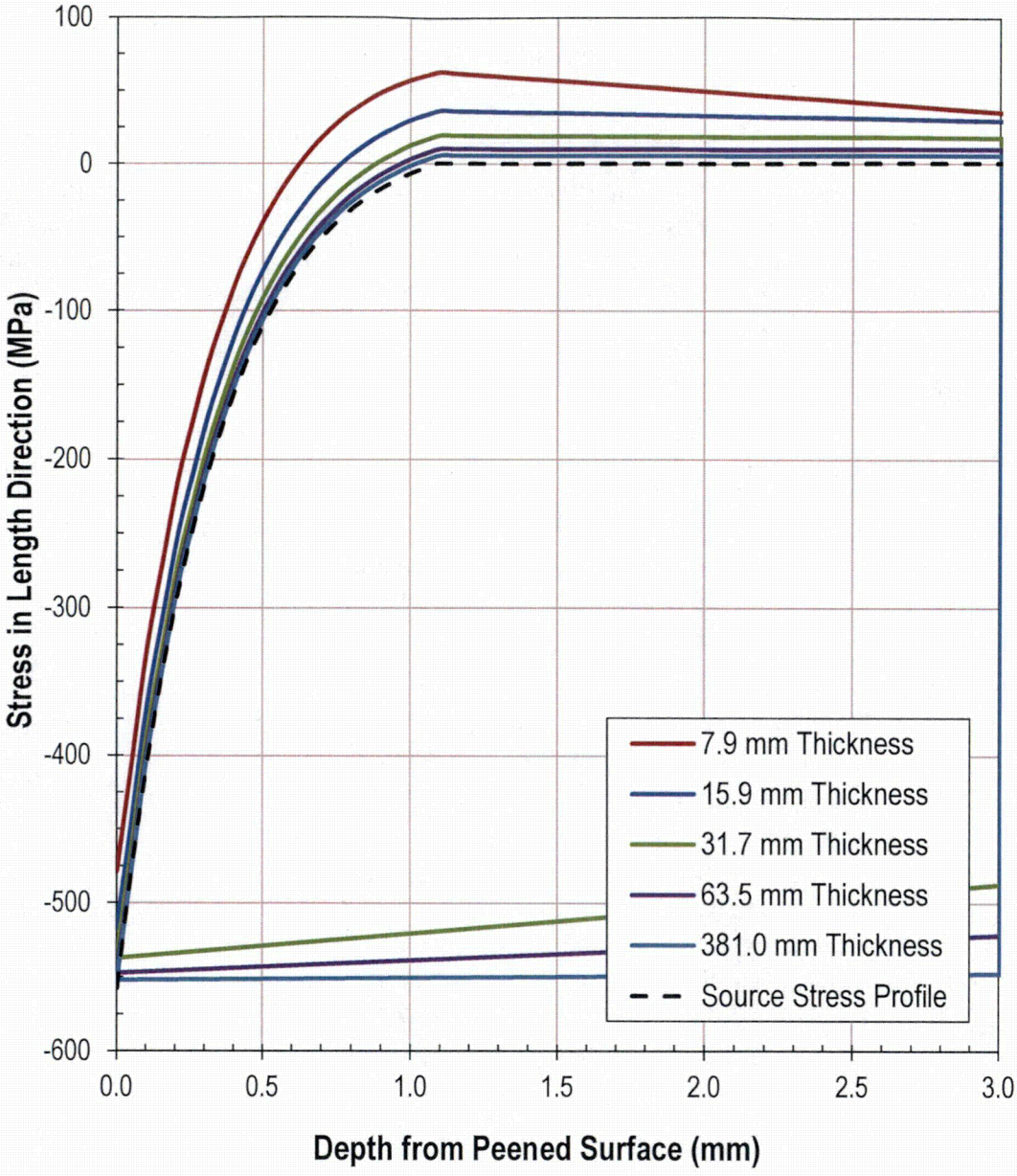

Figure C-5
Equilibrium Through-Wall Stress Profiles for Flat Plate for Common Stress Source Function

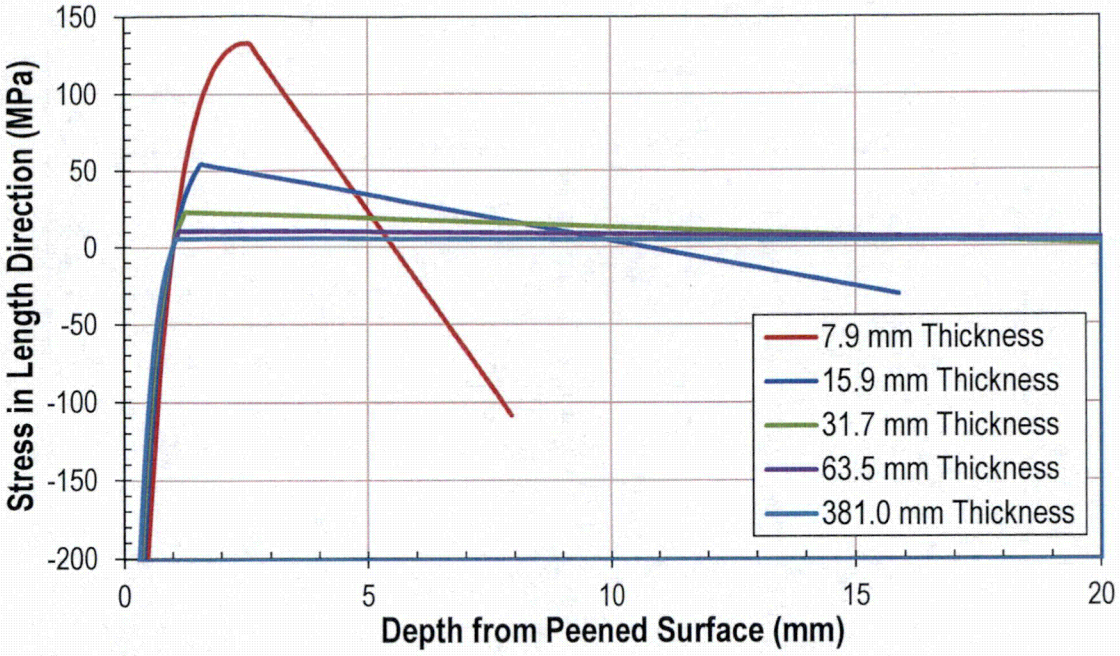

Figure C-6
Effect of Wall Thickness on Through-Wall Stress Profile for Plate Geometry for Same Equilibrium Surface Compressive Stress and Compressive Depth

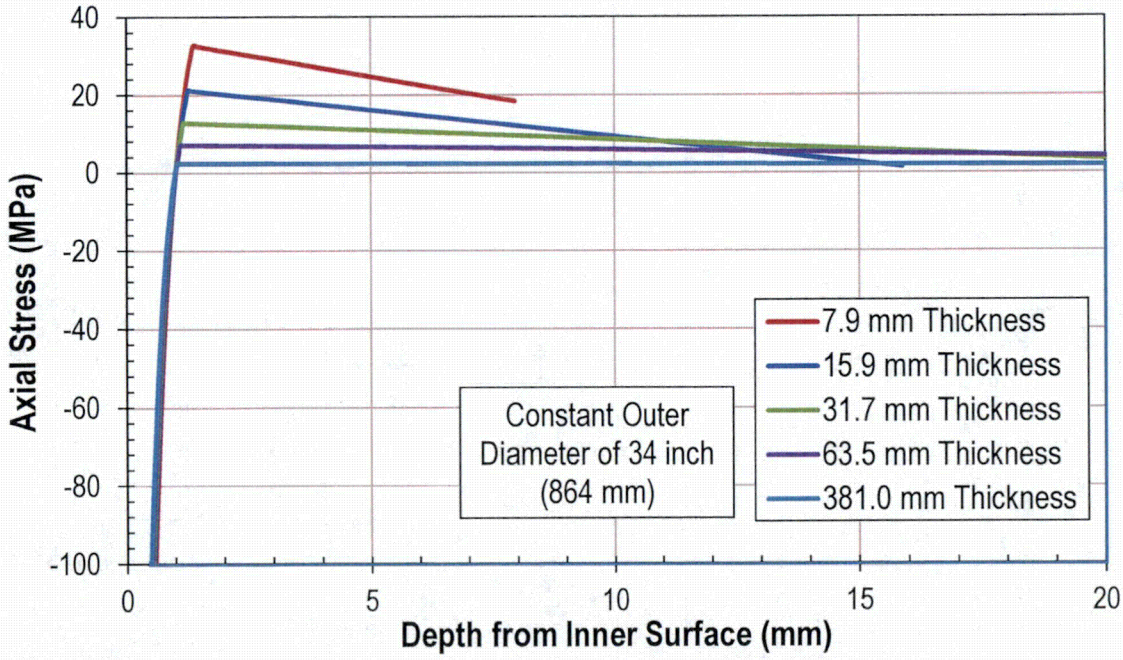

Figure C-7
Effect of Wall Thickness on Through-Wall Axial Stress Profile for Constant Outer Diameter Pipe Geometry for Same Equilibrium Surface Compressive Stress and Compressive Depth

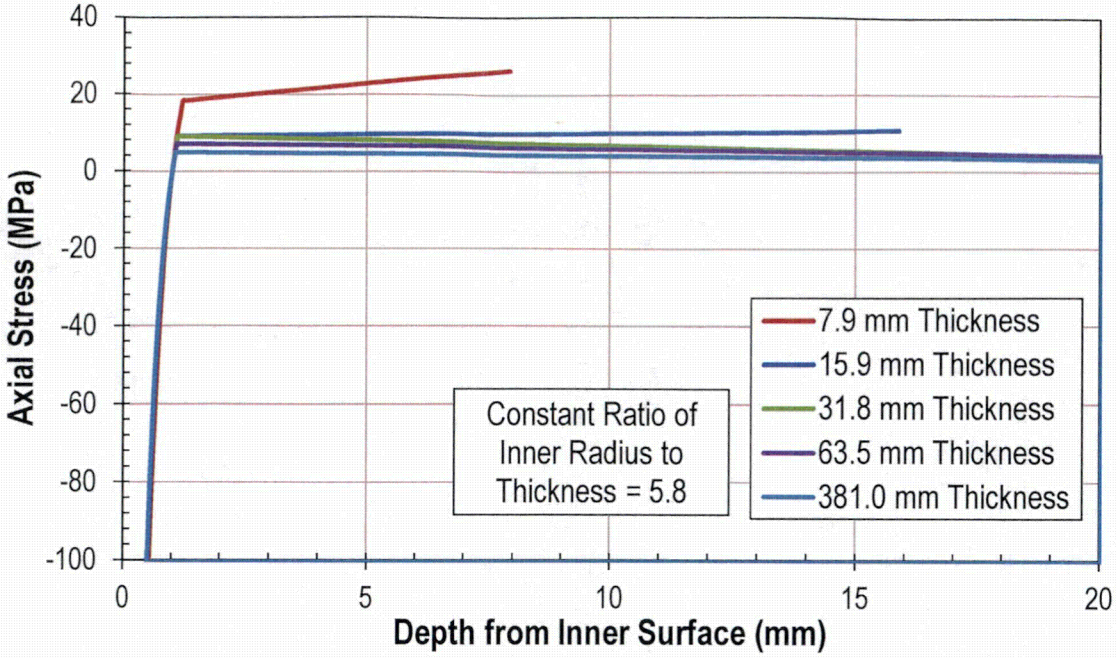

Figure C-8
Effect of Wall Thickness on Through-Wall Axial Stress Profile for Constant R_i / t Pipe Geometry for Same Equilibrium Surface Compressive Stress and Compressive Depth

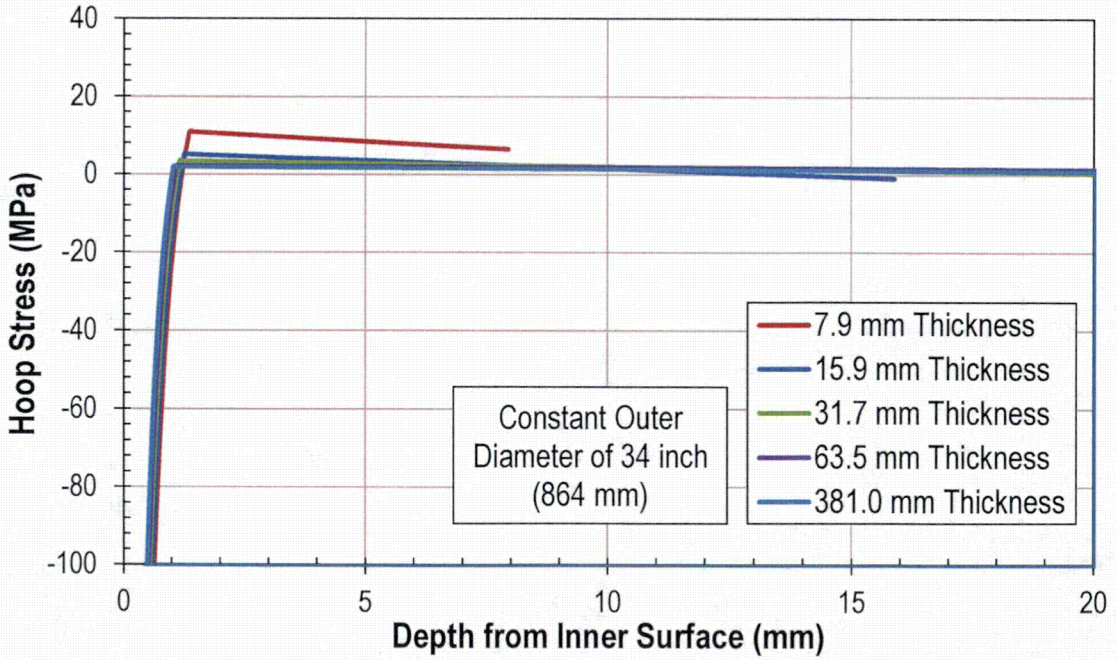

Figure C-9
Effect of Wall Thickness on Through-Wall Hoop Stress Profile for Constant Outer Diameter Pipe Geometry for Same Equilibrium Surface Compressive Stress and Compressive Depth

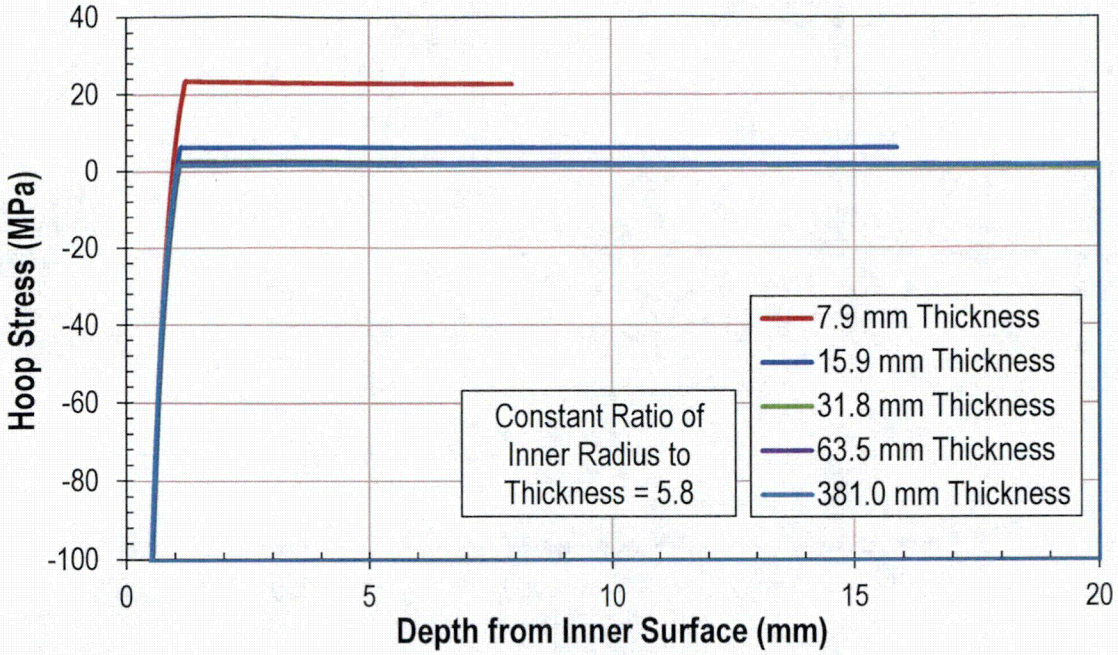

Figure C-10
Effect of Wall Thickness on Through-Wall Hoop Stress Profile for Constant R_i / t Pipe Geometry for Same Equilibrium Surface Compressive Stress and Compressive Depth

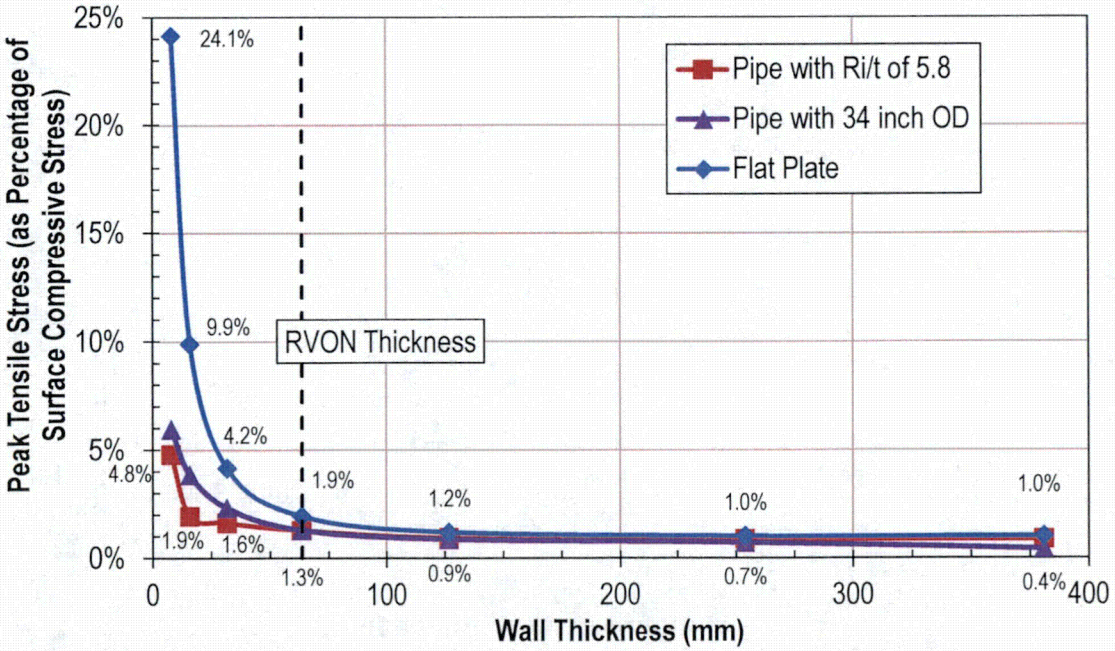

Figure C-11
Effect of Wall Thickness on Peak Tensile Axial Stress for Same Equilibrium Surface Compressive Stress and Compressive Depth

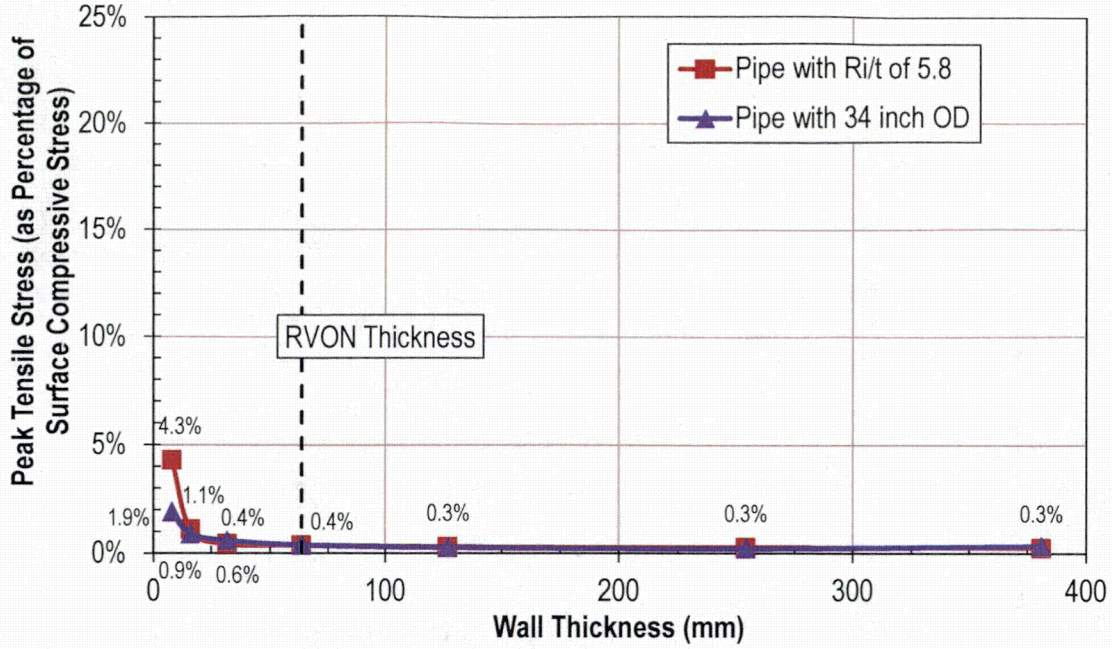

Figure C-12
Effect of Wall Thickness on Peak Tensile Hoop Stress for Same Equilibrium Surface Compressive Stress and Compressive Depth

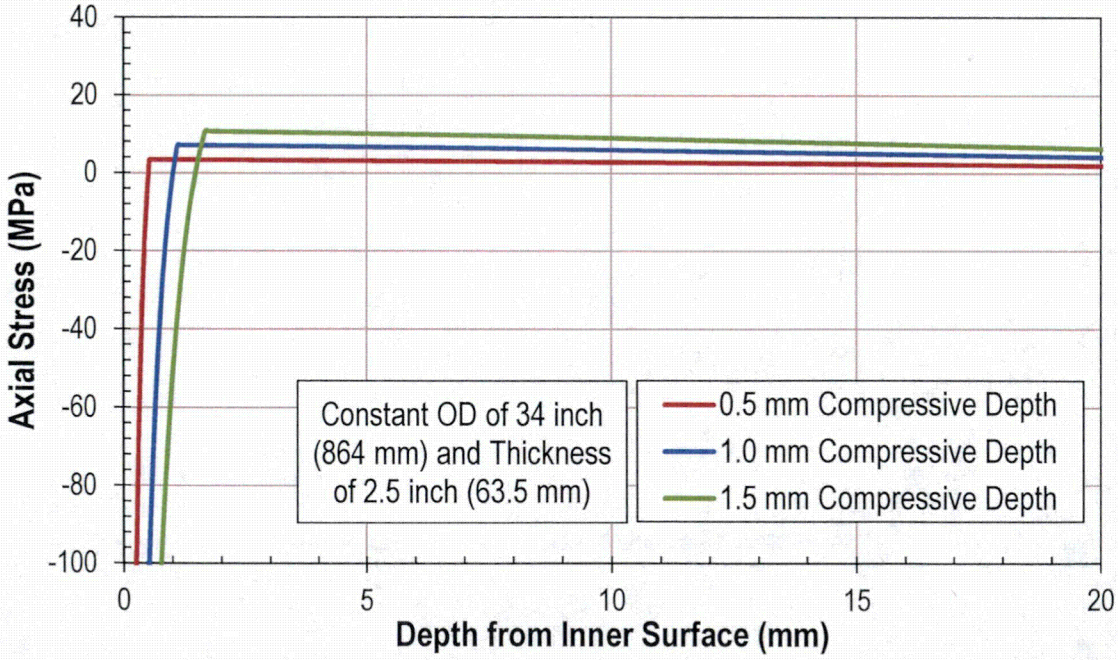

Figure C-13
Effect of Compressive Stress Depth on Through-Wall Axial Stress Profile for RVON Pipe Geometry (Surface Stress Held Constant)

C.5 Model Validation Using Bilinear Stress Profile

The ANSYS model is validated by comparing the resulting stresses to a simple piecewise linear stress profile. The piecewise linear stress profile, which ensures that the applicable force and moment balances are satisfied for the simplest possible profile, is subject to the following assumptions:

1. The profile models the effect of peening only.
2. The compressive surface stress is set to an assumed value, $\sigma(x=0)=\sigma_0$.
3. The stress profile transitions to tensile stresses at a pre-defined point, x_0. This is where $\sigma(x=x_0)=0$.
4. The internal forces must balance to zero through the thickness of the peened component assuming that the profile is uniform over the cross section of an unrestrained flat plate:

$$F_{net}=\int_0^t \sigma(x)dx=0 \qquad \text{[C-3]}$$

5. The internal moments must balance to zero though the thickness of the peened component assuming that the profile is uniform over the cross section of an unrestrained flat plate:

$$M_{net}=\int_0^t x\sigma(x)dx=0 \qquad \text{[C-4]}$$

The piecewise linear stress profile is defined by two line segments; the first is defined by assumptions (2) and (3), whereas the second is defined by assumptions (4) and (5). For the case of the axial stress profile of a thick-wall pipe, Equations [C-3] and [C-4] are assumed to hold except that the force and moment integration are each weighted by the radial coordinate to account for the increase in cross sectional area toward the OD. In each validation case, the values of σ_0 and x_0 were selected to match the FEA profile.

Figure C-14 and Figure C-15 compare the bilinear profile with the FEA results for two cases.

- Figure C-14 shows reasonable agreement versus the FEA solution and measured stress profile for the flat plate case investigated by Hill et al. [5], including similar peak tensile stress values.
- Figure C-15 shows a similar peak tensile stress for the FEA case investigated for a thick-wall pipe with dimensions applicable to reactor vessel outlet and inlet nozzles. The somewhat smaller peak stress for the FEA case is the result of the curvature in the FEA stress profile close to the peened surface. This curvature results in a reduced force and a reduced moment to be balanced by the remainder of the stress profile. This particular FEA stress profile is from a region with a rather uniform curvature that is close to a through-wall moment balance without considering the effect of shear stress on the moment balance.

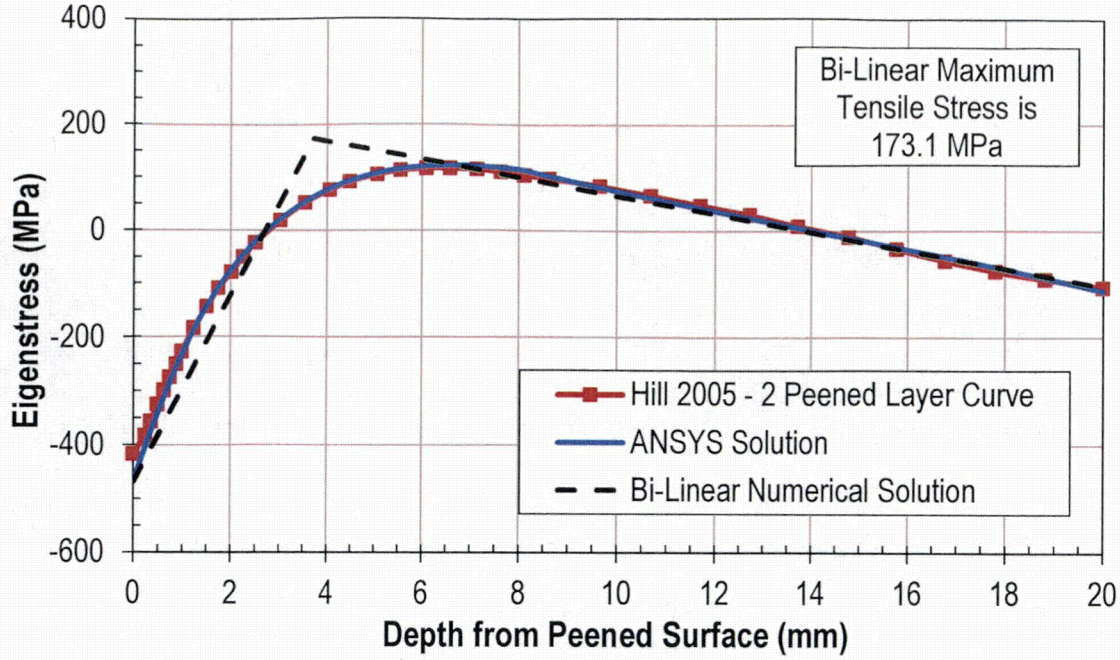

Figure C-14
ANSYS Model Validation for Profile Measured by Hill et al. [5] Using Bilinear Stress Profile

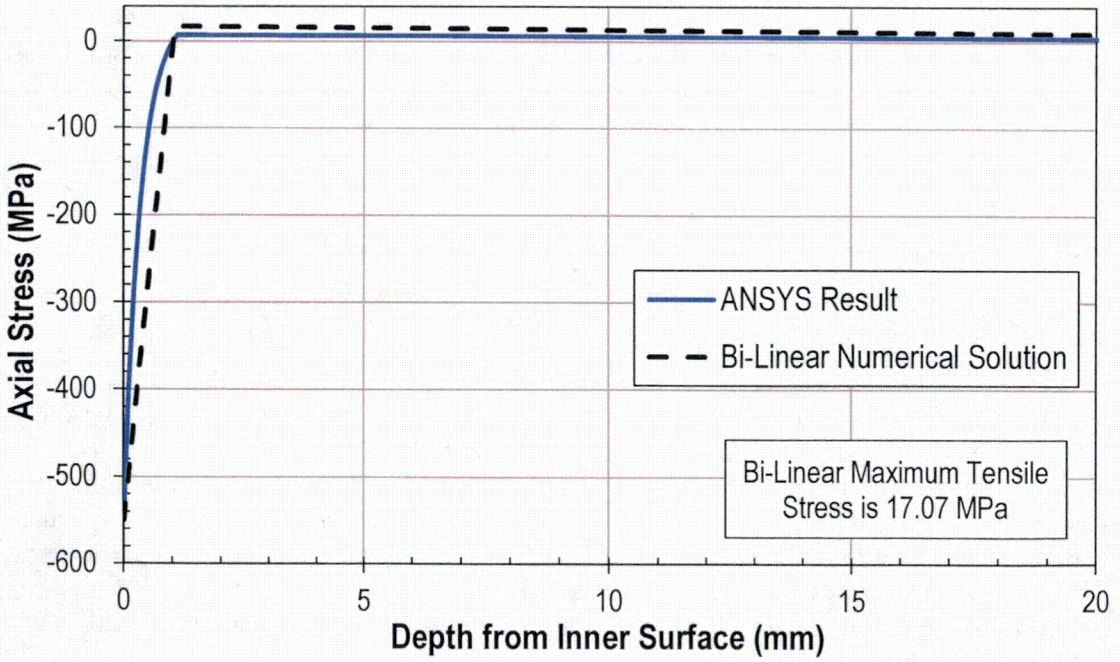

Figure C-15
ANSYS Model Validation for Reactor Vessel Outlet Nozzle (RVON) Case Using Bilinear Stress Profile

C.6 Conclusions

The literature review and analyses presented in this appendix demonstrate the following:

- A balancing stress profile develops beyond the compressive residual stress induced by peening at the treated surface. This balancing stress consists of a through-wall bending component and an axial membrane stress. These residual stress components act to balance the force and change in curvature associated with the peening compressive residual stress developed in the region of the treated surface. The peak tensile stress generally forms in the region just beyond the peening compressive stress layer. The peak tensile stress location represents the location beyond the compressive stress zone where the through-wall bending stress is maximum.
- For a given compressive residual stress effect (surface magnitude and depth of compression) retained upon peening, the peak tensile balancing stress decreases as the component thickness increases. As the component thickness increases, the balancing force and moment are each spread over a greater distance. The difference in balancing stress required to develop the balancing through-wall moment is decreased. The increase in moment arm distance means that a smaller stress difference will create the same moment. Similar trends are produced for thick-wall pipes peened on the inside diameter as for flat plates.
- The peak balancing tensile stress for the case of a peened thick-wall pipe is reduced compared to an unrestrained flat plate of equivalent wall thickness. This is because the more constrained pipe geometry does not deflect as much as the plate case for equivalent peening compressive stress effect and equivalent wall thickness, corresponding to a reduced through-wall drop in the balancing stress profile. The pipe geometry does not satisfy the moment balance in the same manner as for the unrestrained flat plate as shear stresses contribute to the balance for the pipe. The result is that the balancing stress profile for a thick-wall pipe is more nearly uniform than for the case of an unrestrained flat plate of equivalent wall thickness.
- For the reactor vessel outlet nozzle (RVON) geometry evaluated with the FEA model, the peak tensile balancing stresses are less than about 2% of the magnitude of the compressive surface stress for the case of a compressive stress layer at the pipe ID that is 1 millimeter deep. This relatively small magnitude for the peak tensile balancing stress is the result of the balancing force and moment being spread over the large wall thickness of this component, plus the fact that the pipe geometry is more constrained than a flat plate and does not deflect as much as the plate case for equivalent peening compressive stress effect and equivalent wall thickness.

In summary, because of the thick-wall for reactor vessel outlet and inlet nozzles, peening of these components has a small effect on the peak tensile stress below the surface compressive stress zone. With regard to reactor pressure vessel head penetration nozzles (RPVHPNs), the effective thickness of the nozzle at the weld elevation is increased by the presence of the J-groove weld and head. This effect tends to limit the peak tensile balancing stress near the peened ID at the weld elevation. Below the J-groove weld, both the OD and ID surfaces are peened, tending to make the balancing stress uniform over the wall thickness.

C.7 References

1. J. Bernasconi and M. Roth, "The Niku-Lari Method and the Stress Source Method: Application to Residual Stress Distribution of Shot Peened Plates," *Advances in Surface Treatments, Residual Stresses*, Vol. 4, pp. 221-250, Pergamon Press, 1987.
2. S. T. S. Al-Hassani, "Mechanical Aspects of Residual Stress Development in Shot Peening," *Proceedings of ICSP-1*, edited by A. Niku-Lari, pp. 583-602, Pergamon Press, 1981.
3. A. Niku-Lari, "Methode De La Fleche Methode De La Source Des Contraintes Residuelles," *Proceedings of ICSP-1*, edited by A. Niku-Lari, pp. 237-247, Pergamon Press, 1981.
4. D. J. Buchanan and R. John, "Residual Stress Redistribution in Shot Peened Samples Subject to Mechanical Loading," *Materials Science & Engineering A*, Vol. 615, pp. 70-78, 2014.
5. M. R. Hill, et al., "Measurement of Laser Peening Residual Stresses," *Journal of Materials Science & Technology*, Vol. 21, No. 1, pp. 3-9, 2005.
6. R. Menig, et al., "Depth Profiles of Macro Residual Stresses in Thin Shot Peened Steel Plates Determined by X-Ray and Neutron Diffraction," *Scripta Materialia*, Vol. 45, No. 8, pp. 977-983, 2001.
7. A. T. DeWald and M. R. Hill, "Eigenstrain-Based Model for Prediction of Laser Peening Residual Stresses in Arbitrary Three-Dimensional Bodies. Part 2: Model Verification," *Journal of Strain Analysis for Engineering Design*, Vol. 44, No. 1, pp. 13-27, 2009.
8. ANSYS Version 15.0, Mallett Technology, Inc., Canonsbug, PA: 2015.
9. ASME Boiler and Pressure Vessel Code, Section II, Materials, Part D, Properties (Customary), ASME, 2013 Edition, July 1, 2013.
10. *Materials Reliability Program: Alloy 82/182 Pipe Butt Weld Safety Assessment for the US PWR Plant Designs: Westinghouse and CE Design Plants (MRP-109NP)*, EPRI, Palo Alto, CA: 2004. 1009804. [NRC ADAMS Accession No. ML042430093]
11. *Materials Reliability Program: Technical Basis for Primary Water Stress Corrosion Cracking Mitigation by Surface Stress Improvement (MRP-267, Revision 1)*, EPRI, Palo Alto, CA: 2012. 1025839. [Freely Available at www.epri.com]

The Electric Power Research Institute, Inc. (EPRI, www.epri.com) conducts research and development relating to the generation, delivery and use of electricity for the benefit of the public. An independent, nonprofit organization, EPRI brings together its scientists and engineers as well as experts from academia and industry to help address challenges in electricity, including reliability, efficiency, affordability, health, safety and the environment. EPRI also provides technology, policy and economic analyses to drive long-range research and development planning, and supports research in emerging technologies. EPRI's members represent approximately 90 percent of the electricity generated and delivered in the United States, and international participation extends to more than 30 countries. EPRI's principal offices and laboratories are located in Palo Alto, Calif.; Charlotte, N.C.; Knoxville, Tenn.; and Lenox, Mass.

Together...Shaping the Future of Electricity

Program:

Pressurized Water Reactor Materials Reliability Program (MRP)

3002006654

Electric Power Research Institute
3420 Hillview Avenue, Palo Alto, California 94304-1338 • PO Box 10412, Palo Alto, California 94303-0813 USA
800.313.3774 • 650.855.2121 • askepri@epri.com • www.epri.com